One Earth

Article

From decades to years: Rising seas and cyclones amplify Bangladesh's storm-tide hazards in a warming climate

Graphical abstract

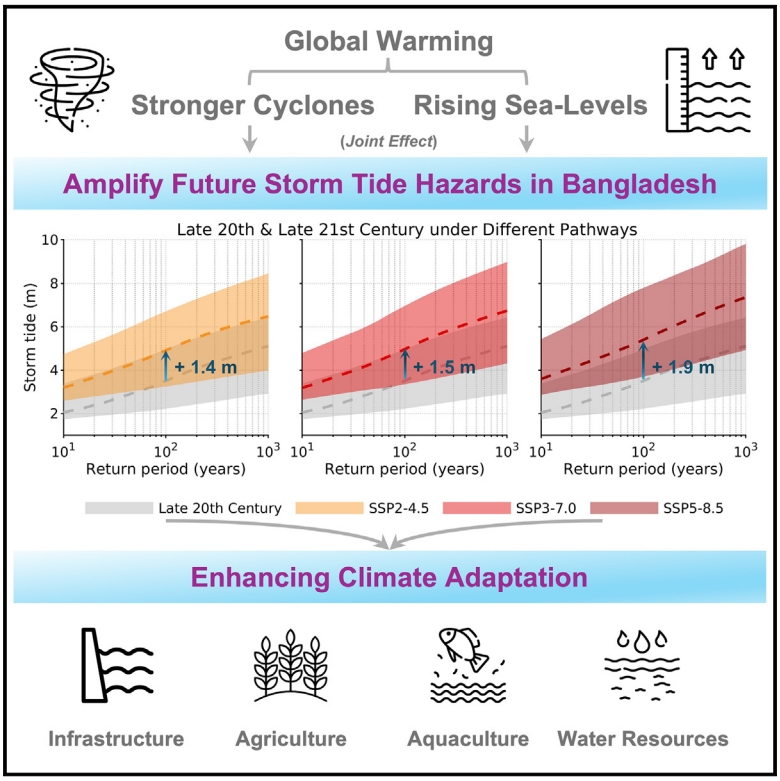

Highlights

- TC climatology change and SLR worsen storm tides in Bangladesh in IPCC AR5 & AR6
- Storm-tide season widens, with peak intensification in late monsoon and post-monsoon
- Cyclone-monsoon cascades and sequential post-monsoon extremes deserve attention
- A joint sampling method integrates TC, SLR, and tides probabilistically in simulations

Authors

Jiangchao Qiu, Sai Ravela, Kerry Emanuel

Correspondence

qiujch24@mit.edu (J.Q.), ravela@mit.edu (S.R.)

In brief

Bangladesh has the world's highest cyclone-induced mortality, yet future risks remain unclear, challenging sustainable development. Here, we present a comprehensive storm-tide risk assessment for Bangladesh using a physics-based approach. Our findings reveal rising risks across emission pathways, with uneven impacts by region and season. This timely assessment offers valuable guidance for climate adaptation, infrastructure planning, and coastal resilience strategies while serving as a valuable tool for other regions facing similar climate threats.

Qiu et al., 2025, One Earth *8*, 101273
April 18, 2025
https://doi.org/10.1016/j.oneear.2025.101273

CellPress

One Earth

CellPress
OPEN ACCESS

Article

From decades to years: Rising seas and cyclones amplify Bangladesh's storm-tide hazards in a warming climate

Jiangchao Qiu,[1,2,*] Sai Ravela,[1,*] and Kerry Emanuel[1]
[1]Department of Earth, Atmospheric and Planetary Sciences, Massachusetts Institute of Technology, 77 Massachusetts, Cambridge, MA 01239, USA
[2]Lead contact
*Correspondence: qiujch24@mit.edu (J.Q.), ravela@mit.edu (S.R.)
https://doi.org/10.1016/j.oneear.2025.101273

SCIENCE FOR SOCIETY Bangladesh's low-lying coast, home to 8 million people, is highly vulnerable to tropical cyclones and storm tides. The government has implemented proactive policies and preparedness programs to enhance the country's resilience and protect against loss of life. However, under a warming climate the sea level will rise and tropical cyclones will intensify, likely elevating the risk of coastal flooding and overwhelming existing flood defenses. In the absence of observational data and powerful computational models, risk assessments adequate to inform infrastructure development are lacking.

Using a physics-based approach that accounts for changes in cyclone activity and sea-level rise, we present a storm-tide hazard risk assessment for Bangladesh under different warming scenarios and reveal an urgent need to update existing coastal defense strategies. Policymakers can use our assessments to enhance resilience, ensuring projects such as the Coastal Embankment Improvement Project and Multipurpose Disaster Shelter Project protect vulnerable communities.

SUMMARY

Rising sea levels and intensifying cyclones threaten Bangladesh's low-lying, densely populated coast in a warming climate, putting millions at risk. Yet future risks remain poorly understood, limiting available guidance for climate adaptation. Here, we present a comprehensive storm-tide risk assessment for Bangladesh using a coupled statistical-physical downscaling and hydrodynamic framework that integrates projected cyclone activity and sea-level rise across multiple climate scenarios. Our scalable large-ensemble multimodel approach reveals a significant and previously unrecognized 10-fold drop in average late-century storm-tide return periods under middle- to high-emission pathways, with notable regional and seasonal variations. Two emerging risks require urgent attention: cascading cyclone-monsoon hazards in the late monsoon and sequential extremes in the post-monsoon. Our findings index storm-tide hazard estimates to climate scenarios to inform policymakers and planners on climate adaptation, infrastructure planning, and resilience strategies, and underscore the need to reassess ongoing coastal protection efforts.

INTRODUCTION

Tropical cyclone (TC)-induced coastal floods rank among the deadliest and costliest worldwide catastrophes.[1] The Bay of Bengal (BoB), located in the northeastern part of the Indian Ocean, has experienced some of the most destructive coastal floods in history. Although it accounts for only 5%–6% of global TC activity, approximately 80%–90% of global TC fatalities occur in this basin.[2,3] The BoB's funnel-shaped and shallow northern region naturally amplifies the water level, raising it to 10 m above mean sea level when strong TCs strike.[4,5] Six TCs in the BoB have each caused more than 140,000 fatalities,[1] primarily due to coastal flood inundation of the low-lying (less than 5 m above mean sea level), densely populated mega-delta (with a population density of 6,734 per km^2).[6]

Bangladesh is a downstream riparian state for three major trans-Himalayan rivers, namely the Ganges, the Brahmaputra, and the Meghna, and is fringed by the BoB. It has a history of devastation caused by TCs, with 14 events each resulting in the loss of over 10,000 lives from 1760 to 2020.[7] The latest of these was cyclone Gorky in April 1991, which claimed at least 140,000 lives. Sitting on the frontline in the battle against coastal floods,

Please cite this article in press as: Qiu et al., From decades to years: Rising seas and cyclones amplify Bangladesh's storm-tide hazards in a warming climate, One Earth (2025), https://doi.org/10.1016/j.oneear.2025.101273

Bangladesh has since emerged as an international champion for improved coastal defenses,[8] implementing proactive policies to improve its resilience significantly. The government has improved its early warning system, increasing access to a network of cyclone shelters and evacuation roads, improving polders (low-lying areas surrounded by embankments), and implementing community-based cyclone preparedness programs.[9] These efforts have yielded impressive results, reducing mortality from TCs by nearly a hundredfold. In May 2020, super cyclone Amphan, rapidly intensifying to Category 4 within six hours, hit the western coast of Bangladesh, resulting in a limited death toll of 128 despite inducing a 5-m storm surge.[10]

However, a warming climate likely poses a significant threat to Bangladesh. The polder embankment systems, which consist of 139 polders covering 1.2 million hectares of land, were built to protect about 8 million people from flooding and ensure their safety and livelihoods.[9] If sea-level rise (SLR) and extreme TCs become more frequent and destructive due to climate change, the exposed infrastructure and vulnerable populations will be at greater risk. Increased sedimentation, elevating riverbeds, and land subsidence within polders increase embankment stress exposure to even low-intensity TCs.[11] Furthermore, rising coastal water levels, reduced upstream river discharge, and polder-induced tidal amplification may worsen salinity intrusion.[12] If the cyclone season expands into the monsoon season, the combined impact of coastal and inland flooding could devastate agriculture and water supply, further straining the vulnerable population.

The consequences faced by coastal Bangladesh are severe and often appear irreversible. In light of the emerging climate hazard, Bangladesh's coastal architecture seems fragile and unsustainable. Risk-informed solutions are needed, so it is necessary to quantify climate change impacts accurately. While revisions entailing coastal planning are most immediate in Bangladesh, as a representative low-lying coastal delta, methods to quantify risk accurately are likely to apply to many other regions facing similar threats such as Mozambique,[13,14] the Philippines,[15,16] Myanmar,[17] Vietnam,[18,19] and southern China.[20–22]

In the context of TC-induced storm-surge risk, downscaling TCs to establish climatologies in future climate scenarios holds promise for quantifying the hazard. However, it is challenging to do so using the limited observational record of cyclones passing through Bangladesh or bearing the enormous computational expense of running high-resolution numerical climate models. To address these limitations, synthetic TC models have become a valuable tool for risk assessment.[23–28] Emanuel et al.'s statistical-physical downscaling framework, in particular, has proven effective in regions with sparse observational data and under future climate scenarios.[23,24] Although researchers have used the framework in other regions,[18,29–31] few have extended these methods to the BoB, which limits Bangladesh's ability to adapt effectively to escalating climate risks.

In the BoB, a historical multimodel intercomparison study[32] demonstrated the superior performance of this approach, in contrast to purely statistical models such as STORM (Synthetic Tropical Cyclone Generation Model),[26] which tend to overestimate high-intensity TCs due to data limitations. Further, while studies have applied Emanuel et al.'s framework to assess storm-tide risks in Bangladesh,[33] the assessments are confined to the current climate. Emanuel[7] indicates that under a high-greenhouse-gas-emissions scenario, the likelihood of extreme TC winds (exceeding 77 m/s [150 knots]) could increase 10-fold by the end of the century. Despite these alarming findings, no studies have examined TC-induced storm-tide risks for Bangladesh under changing climate scenarios, leading to a critical knowledge gap.

Here, to overcome this critical knowledge gap, we present a comprehensive storm-tide risk assessment for Bangladesh. We explicitly and efficiently downscale TCs and simulate storm tides across coastal Bangladesh under projected climate scenarios by applying a statistical-physical framework.[23,24] Our approach reveals a significant 10-fold drop in average late-century storm-tide return periods under middle- to high-emission pathways, with notable regional and seasonal variations. The findings provide policymakers and stakeholders with actionable insights that enhance coastal resilience based on the magnitude, timing, and location of hazards. These efforts can strengthen adaptation of communities in Bangladesh's coastal regions and may provide critical and timely updates to ongoing efforts such as the Coastal Embankment Improvement Project (CEIP).[34] While our study focuses on Bangladesh, the coupled statistical-physical downscaling and hydrodynamic framework can also be applied to other low-lying regions facing similar threats and urgently requiring tools to enhance risk assessments and strengthen resilience planning in a changing climate, such as South China, Southeast Asia, East Africa, and northeastern Australia.

RESULTS

Methods summary

The coupled downscaling and hydrodynamic framework involves three primary components: synthetic TC downscaling, hydrodynamic simulation of storm tides, and statistical analysis incorporating bias correction. A brief description of the workflow using these components is as follows. We use a downscaled synthetic TC track set[7] to investigate the effects of climate change (including TC climatology change and probabilistic SLR) on Bangladesh's storm tides. Simulated synthetic TCs drive a verified hydrodynamic model[35] to simulate storm tides, dynamically incorporating astronomic tides and SLR using updated higher-accuracy regional bathymetry.[33,36]

The simulated hydrodynamic storm-tide ensemble provides the results in this paper. Specifically, we estimate storm-tide return periods in present climate and future climate scenarios, including the combined effect of future TC climatology change and SLR. We then investigate storm-tide distributions across seasons for severity and frequency. We additionally analyze the frequency that storms similar to the historically deadliest TC-induced storm tides (Bhola and Gorky: tracks and fatalities can be found in Figure 1) might have in a warming climate.

Storm-tide hazards in current and future scenarios

We conducted storm-tide hazard assessments in Bangladesh to evaluate the impacts of climate change on storm tides and identify the most vulnerable regions. These assessments span national (aggregate projections from all 50 "virtual stations" [VSs]), regional (projections aggregated for VSs in the Ganges,

Please cite this article in press as: Qiu et al., From decades to years: Rising seas and cyclones amplify Bangladesh's storm-tide hazards in a warming climate, One Earth (2025), https://doi.org/10.1016/j.oneear.2025.101273

CellPress
OPEN ACCESS

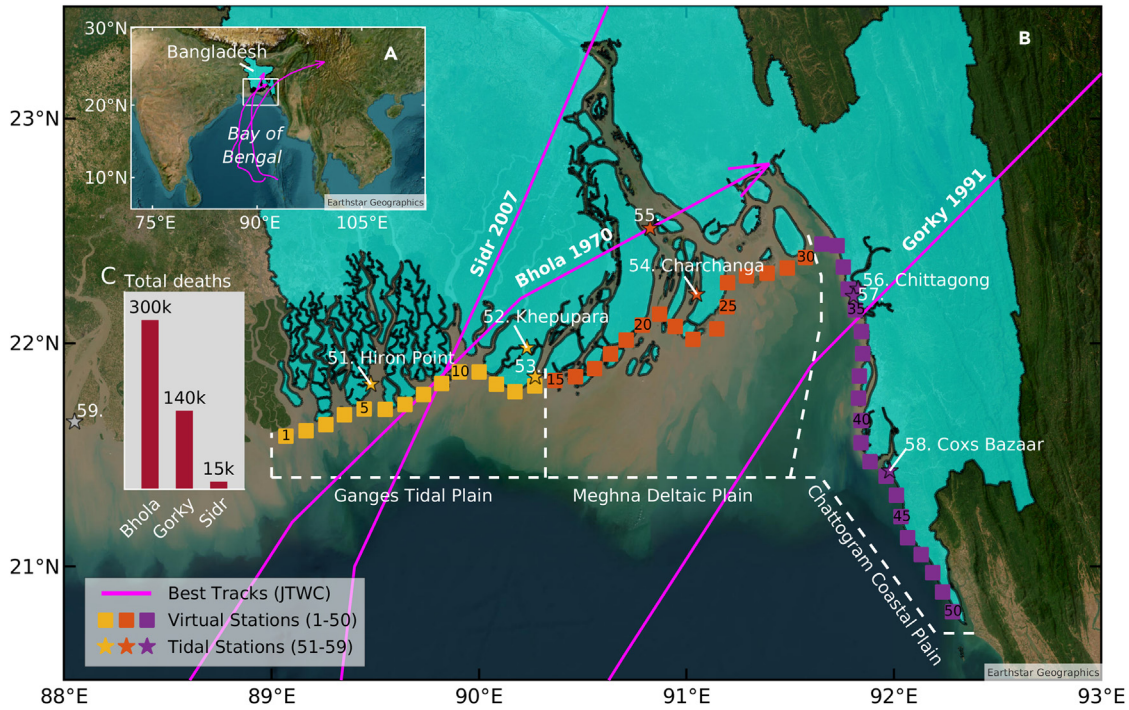

Figure 1. Maps of historically deadliest TCs that made landfall in Bangladesh

(A) The Joint Typhoon Warning Center (JTWC) tracks Bhola (1970), Gorky (1991), and Sidr (2007) TCs, marking them in magenta with arrows. These cyclones originate in the BoB and move northward to strike Bangladesh, highlighted in cyan.

(B) The map zooms into coastal Bangladesh to show where these three TCs made landfall and identifies 58 water-level stations across Southwest Bangladesh (Ganges Tidal Plain, marked yellow), Middle Bangladesh (Meghna Deltaic Plain, marked orange), and East Bangladesh (Chattogram Coastal Plain, marked purple). The equidistant sampling divides Bangladesh's 300-km coastline into 50 points (defined as "virtual stations [VS]") spaced 6 km apart. These points supplement the limited existing tidal stations. The map labels VSs with names of MIT/Earth Signals and Systems Group alums, representing them as squares with IDs from 1 to 50, while pentagrams represent tidal stations with IDs from 51 to 59. Table S1 provides detailed information on these regional stations.

(C) The histogram associates each reported total fatality count with the corresponding TC (data from Needham et al.[1]). The base map integrates data from BDP 2100 (Baseline Volume 1, page 403), Humanitarian Data Exchange, World Bank, ESRI ArcGIS, Maxar, Earthstar Geographics, USDA FSA, USGS, Aerogrid, IGN, IGP, and the GIS user community.

Meghna, and Chattogram regions), and local (station-specific) scales.

At the national scale, we find that climate change will significantly increase Bangladesh's storm tides by the end of the 21st century, even under moderate scenarios (see Figure S1). The projected increases in storm-tide risk under the CMIP6 SSP2-4.5 and SSP3-7.0 scenarios are similar in magnitude, regardless of whether SLR is included, but remain lower than those under the SSP5-8.5 scenario. Statistical uncertainty also grows at extended return periods. Specifically, the 100-year storm tide, currently estimated at 3.5 m (confidence interval [CI] 2.2–5.0 m), is projected to rise to 4.9 m (CI 3.2–6.7 m) under SSP2-4.5, 5.0 m (CI 3.4–6.9 m) under SSP3-7.0, and 5.4 m (CI 3.7–7.8 m) under SSP5-8.5.

Including TC climatology changes and SLR yields median increases of 1.4 m, 1.5 m, and 1.9 m under SSP2-4.5, SSP3-7.0, and SSP5-8.5, respectively. Excluding SLR, TC climatology changes alone will increase storm tides by 0.6 m, 0.6 m, and 0.9 m under the exact scenarios. Additionally, we assessed storm-tide changes under CMIP5 RCP4.5 and RCP8.5 scenarios (see Figure S4), finding that CMIP6 projections indicate a higher risk than CMIP5 projections (see discussion).

At the regional scale (see Figure 2), storm-tide impacts are uneven across Bangladesh. Northern Chattogram is the most vulnerable region, followed by Meghna and Ganges, with southern Chattogram ranking fourth. The 100-year storm tides for the Ganges, Meghna, and Chattogram are projected to increase by 1.4 m, 2.0 m, and 1.1 m (medians), respectively, under SSP2-4.5; by 1.4 m, 2.3 m, and 1.2 m (medians) under SSP3-7.0; by 1.9 m, 2.8 m, and 1.7 m (medians) under SSP5-8.5.

Further dividing Chattogram into northern (see VS IDs 31–37 in Figure 1) and southern segments (see VS IDs 38–50 in Figure 1), we find that northern Chattogram experiences more significant increases, with median rises of 1.5 m, 1.5 m, and 2.3 m under SSP2-4.5, SSP3-7.0, and SSP5-8.5, respectively. In contrast, the southern Chattogram shows smaller median increases of 1.0 m, 1.2 m, and 1.6 m under the exact same scenarios. Similar regional assessments under CMIP5 RCP4.5 and RCP8.5 scenarios are presented in Figures S5 and S6.

At the local scale (station-specific; see Figure 3), we observe that increases under SSP5-8.5 are more pronounced than under SSP2-4.5 and SSP3-7.0. The most substantial storm-tide increases occur at stations in northern Chattogram. For example, at VS Navi (ID 31) in northern Chattogram, the 100-year storm tide is projected to increase by 1.8 m, 1.9 m, and 2.7 m (medians) under SSP2-4.5, SSP3-7.0, and SSP5-8.5, respectively. In comparison, at VS Zhuchang (ID 49) in southern Chattogram, the

Please cite this article in press as: Qiu et al., From decades to years: Rising seas and cyclones amplify Bangladesh's storm-tide hazards in a warming climate, One Earth (2025), https://doi.org/10.1016/j.oneear.2025.101273

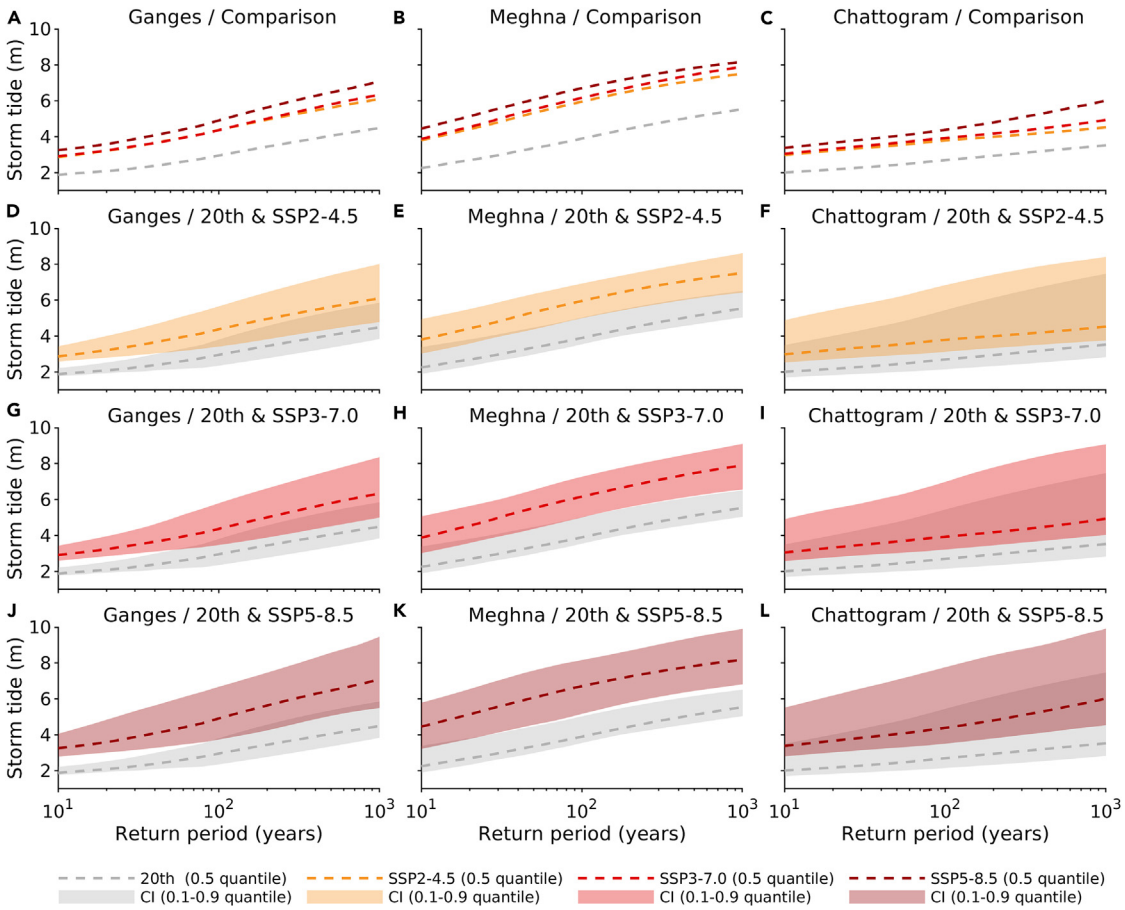

Figure 2. Bangladesh's storm tides versus return periods while considering SLR, as projected by CMIP6 models at the regional scale

(A, D, G, and J) Projections for the Ganges.

(B, E, H, and K) Projections for the Meghna.

(C, F, I, and L) Projections for the Chattogram.

(A–C) Comparison between the current climate and the future CMIP6 SSP2-4.5, SSP3-7.0, and SSP5-8.5 climates.

(D–F) CMIP6 model ensembles under the SSP2-4.5 scenario.

(G–I) CMIP6 model ensembles under the SSP3-7.0 scenario.

(J–L) CMIP6 model ensembles under the SSP5-8.5 scenario.

Storm tides are the total water levels (combined components of astronomic tide, storm surge, and mean sea-level state) relative to the mean sea level of the 1995–2014 baseline. Dashed lines indicate the ensemble median (0.5 quantiles), while shaded areas indicate each estimate's confidence interval (CI, 0.1–0.9 quantiles). The current climate period spans from 1981 to 2000, while the future climate period spans from 2081 to 2100. The CIs account for variability in tide, SLR, TCs, climate models, multiple-station data, and kernel-GPD parameters.

increases are 1.0 m, 1.1 m, and 1.6 m (medians) under the exact scenarios.

Storm tides driven solely by TC climatology changes (Figure S3) under SSP3-7.0 show slightly smaller increases than those under SSP2-4.5, as considered further in the discussion.

SLR and TC contributions to storm tides

Two primary factors influence the changes in the storm tide: TC climatology changes and SLR. However, their roles differ across Bangladesh's coastline. As depicted in Figure 4, projections under CMIP6 SSP5-8.5 indicate that TC climatology change contributes more to storm tide than SLR, with TC contributions exceeding 50%. Moreover, the proportion of the storm tide attributed to TC climatology change is more significant under SSP5-8.5 compared to SSP2-4.5 and SSP3-7.0. The assessments compare the ensemble medians of storm tide with SLR incorporated (Figure 3) and without SLR incorporated (Figure S3) for each return period. The SLR case injects stochastic time-dependent SLR in storm-tide simulations (see methods and Figures S22–S24).

Specifically, using the 100-year storm tide as an example (Figures 4D–4F), under SSP2-4.5, 44% of all 50 VSs experience an increase predominantly caused by TC climatology change rather than SLR. Similarly, under SSP3-7.0, TC climatology change contributes more than SLR to the rise in 26% of all 50 VSs. In comparison, projections under SSP5-8.5 indicate that TC climatology changes dominate the growth in 74% of all 50 VSs. Table S6 summarizes the average contribution of TC climatology change to the increase in 100-year storm tides in the Ganges, Meghna, and Chattogram under various scenarios.

Please cite this article in press as: Qiu et al., From decades to years: Rising seas and cyclones amplify Bangladesh's storm-tide hazards in a warming climate, One Earth (2025), https://doi.org/10.1016/j.oneear.2025.101273

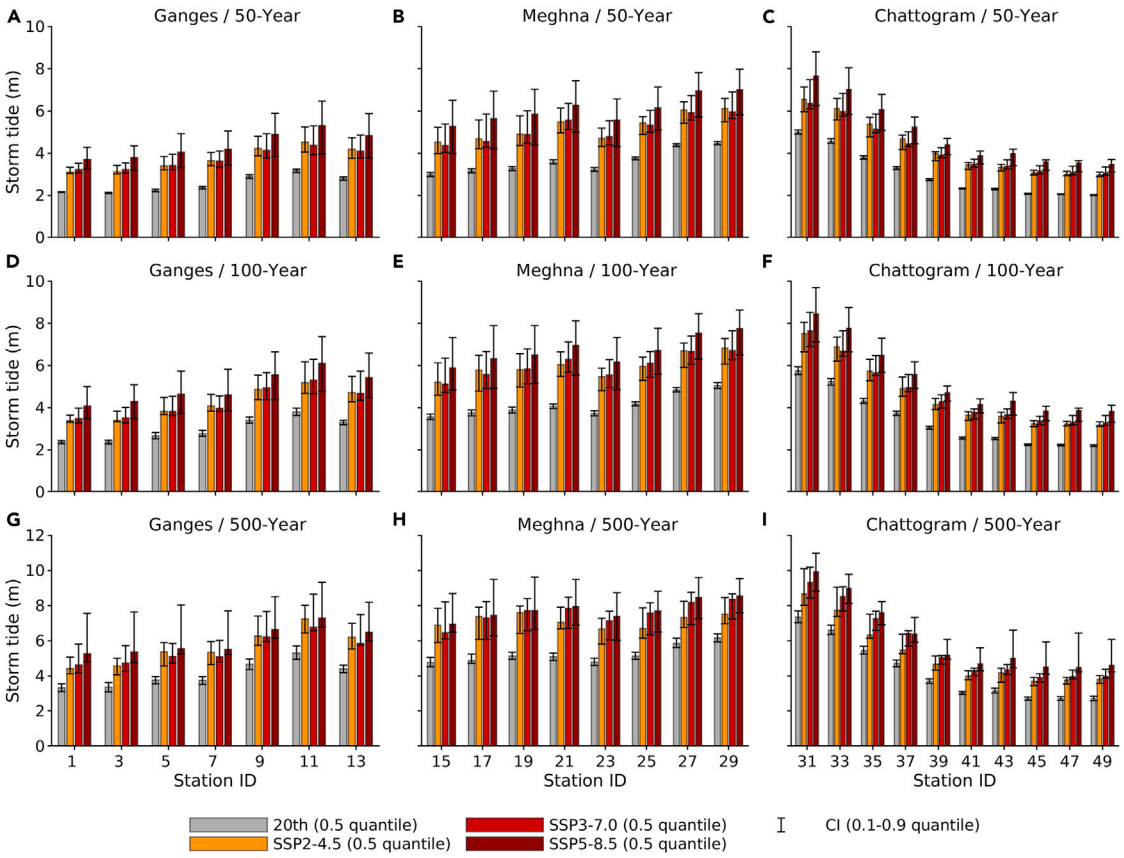

Figure 3. Bangladesh's 50-, 100-, and 500-year storm tides while considering SLR, as projected by CMIP6 models at the station scale

(A–C) 50-year return period.

(D–F) 100-year return period.

(G–I) 500-year return period.

(A, D, and G) Stations located in the Ganges (southwest Bangladesh).

(B, E, and H) Stations located in the Meghna (middle Bangladesh).

(C, F, and I) Stations located in the Chattogram (east Bangladesh).

Storm tides are the total water levels (combined components of the astronomic tide, storm surge, and mean sea-level state) relative to the mean sea level of the 1995–2014 baseline. Projections at all 58 stations are available, but the graph displays only every other station (VS). Histogram heights indicate the ensemble median (0.5 quantiles) for the current climate, CMIP6 SSP2-4.5, SSP3-7.0, and SSP5-8.5 climates. Vertical error bars indicate each estimate's confidence interval (CI, 0.1–0.9 quantiles). The current climate period spans from 1981 to 2000, while the future climate period spans from 2081 to 2100. The CIs account for variability in tide, SLR, TCs, climate models, and kernel-GPD parameters.

The future risk of historically deadliest storms

Estimating the annual exceedance frequency (the reciprocal of the return period) of storm tides in future scenarios similar to the deadliest TCs from the past, such as TC Bhola (1970) and TC Gorky (1991), is crucial for communicating the potential dangers of climate change to the public and developing effective climate adaptation strategies. Overall, our large-ensemble multi-model assessment spanning stations, return periods, and scenarios reveals a 10-fold drop in average late-century storm-tide return periods under middle- to high-emission pathways, indicating a corresponding 10-fold increase in risk.

Figure 5 illustrates the annual frequency of these two deadliest TC-induced storm tides in the current climate and their potential change in a warming climate, considering the joint effect of TC climatology change and SLR. The projected annual frequency increases significantly: 7–18 times for the Bhola-like TC and 6–23 times for a Gorky-like TC, respectively. We note that the Meghna estuary region is more susceptible to extreme storm tides, as the Bhola and Gorky cyclones produced maximum storm tides of similar magnitudes but significantly different return periods at two different locations. This fact underscores the need for heightened attention and preparedness in this region.

Assessing the risk of historic events across the entire coastline is challenging due to poor monitoring of water-level records. Only limited observations document the maximum storm tide with explicit vertical datum information during Bhola (6.1 m above mean sea level, observed at Northern Bhola Island)[37] and Gorky (6.2 m above mean sea level, observed at a location near the Karnaphuli River mouth),[38] respectively. We examine the 55th and 57th stations (which are nearest to the observations) to approximately represent Bhola-induced and Gorky-induced maximum storm tides, respectively. Table S7 summarizes the projected return periods.

Please cite this article in press as: Qiu et al., From decades to years: Rising seas and cyclones amplify Bangladesh's storm-tide hazards in a warming climate, One Earth (2025), https://doi.org/10.1016/j.oneear.2025.101273

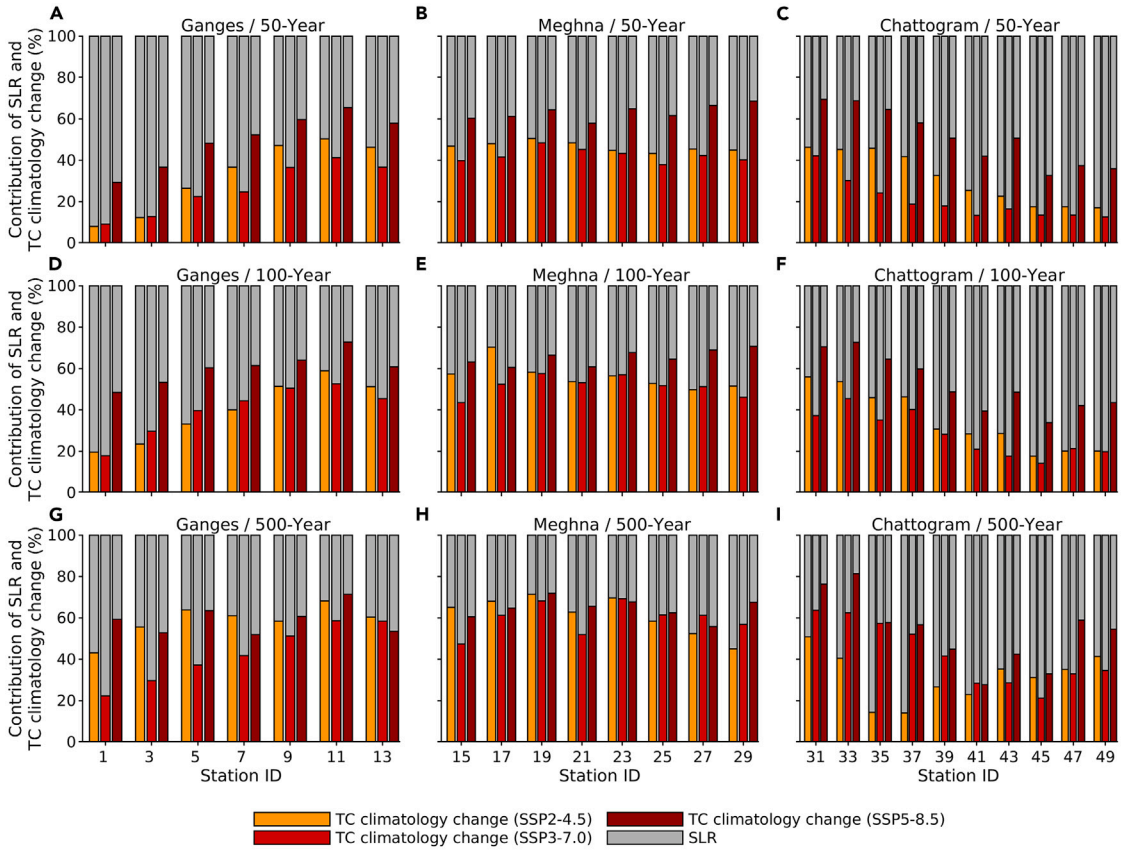

Figure 4. Contribution of TC climatology change and SLR to changes in Bangladesh's storm tides (50-, 100-, and 500-year return periods) at the station scale

(A–C) 50-year return period.
(D–F) 100-year return period.
(G–I) 500-year return period.
(A, D, and G) Stations located in the Ganges.
(B, E, and H) Stations located in the Meghna.
(C, F, and I) Stations located in the Chattogram.
While projections for all 58 stations are available, the graph displays only every other VS. The stacked histogram heights indicate the contributions of TC climatology change and SLR to storm-tide changes projected under the CMIP6 SSP2-4.5, SSP3-7.0, and SSP5-8.5 climate scenarios, respectively. The changes in storm tide are calculated based on the ensemble median (0.5 quantiles). We assess the contributions of TC climatology change and SLR over the future period (2081–2100) compared to the baseline period (1981–2000).

Shifting seasonal severity and frequency regimes

Bangladesh's landfalling TCs exhibit a clear bimodal seasonality, with activity peaks during the pre-monsoon period (April–May) and the post-monsoon period (October–December). These periods are separated by a relatively silent phase from June to August, attributed to the strong vertical wind shear caused by the South Asian summer monsoon.[39]

To explore how climate change may impact these seasonal storm-tide regimes, we analyze changes in storm-tide severity and frequency. Figure 6 highlights shifts in severity, while Figure 7 focuses on frequency alterations across various climate scenarios.

Our findings indicate that climate change significantly amplifies Bangladesh's extreme storm tides. In Figures 6A–6D, ensemble projections suggest that the most dangerous storm tides still occur during the pre-monsoon and post-monsoon seasons. Climate change appears likely to shorten the interval of cyclone dormancy from 75 days (±7 days around August 1, August 15, September 1, December 1, and December 15) to a mere 15 days (±7 days around August 1). Moreover, destructive storm tides expand seasonally in nearly all scenarios and significantly, with severity amplifying most within both the late summer monsoon (±7 days around August 1, August 15, and September 1) and late post-monsoon (±7 days around December 1 and December 15) seasons. In Figure 6E, the severity ratios increase significantly during the late summer monsoon season and the late post-monsoon season compared to any other time. Table S8 summarizes the projected storm-tide severity and increased ratios.

Although our analysis focuses solely on storm tides, the overlap between heightened water levels during the late monsoon season (mid-August) and potentially heavy monsoon rainfall (e.g., the devastating floods of August 2017[40] and July 2020[41]) can significantly amplify cascading inland-coastal flood risks in

Please cite this article in press as: Qiu et al., From decades to years: Rising seas and cyclones amplify Bangladesh's storm-tide hazards in a warming climate, One Earth (2025), https://doi.org/10.1016/j.oneear.2025.101273

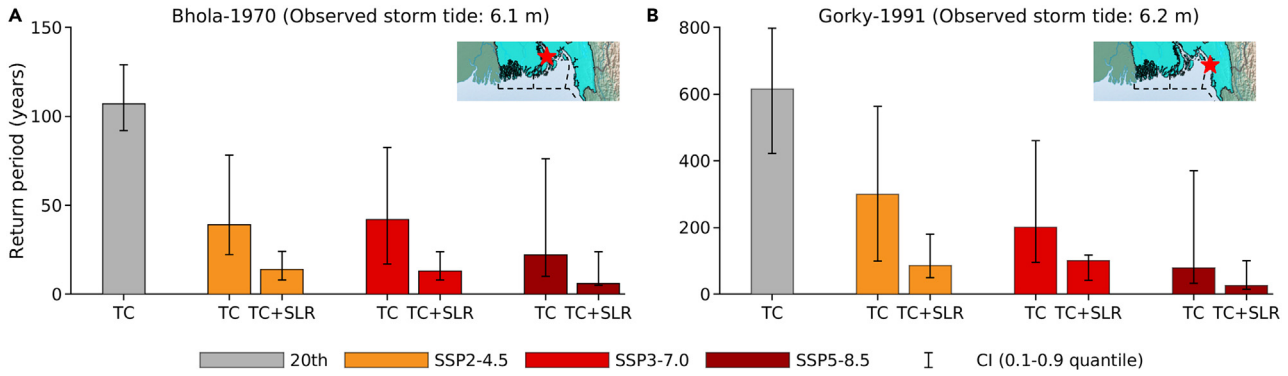

Figure 5. Changing annual frequency of storm tides similar to historically deadliest TCs in a warming climate

(A) Assessment for TC Bhola at station Northern Bhola Island (ID 55).

(B) Assessment for TC Gorky at station Anwara (ID 57, near the Karnaphuli River mouth).

The histogram height represents the ensemble median for the estimated return period of storm tide corresponding to the observed peak storm tide (based on local mean sea level, sourced from previous studies[37,38]). The whiskers indicate the estimated confidence interval (CI, 0.1–0.9 quantiles). The red pentagram icon in the top-right corner of each subplot marks the location of the maximum measured storm tide during the two landfall TCs. The CIs account for variability in tide, SLR, TCs, climate models, and kernel-GPD parameters. The effects of wave setup and river discharge on observed historical extreme water levels are poorly documented and assumed to be non-significant for this hazard assessment. Our large-ensemble multimodel assessment (across stations, return periods, and scenarios) reveals a 10-fold drop in average late-century storm-tide return periods, accounting for TC climatology changes and SLR under middle- to high-emission pathways, indicating an average 10-fold increase in risk. Base map sourced from the BDP 2100 (Baseline Volume 1, page 403), Humanitarian Data Exchange, World Bank, ESRI ArcGIS, Maxar, Earthstar Geographics, USDA FSA, USGS, Aerogrid, IGN, IGP, and the GIS user community.

Bangladesh—the risk is further compounded considering additional flooding from TC-induced rainfall.

During the first cyclone dormancy period (July 25 to September 8), projections under SSP2-4.5 and SSP3-7.0 indicate that even the minimum storm tide (5.8 m) in warming climates exceeds the maximum storm tide (4.2 m) under the current climate. The second cyclone dormancy period (November 24 to December 22) shows a similar phenomenon. However, under the high-emission SSP5-8.5 scenario, a pronounced seesaw effect emerges: the highest storm tide during the first dormancy period decreases to just 3.3 m, while the second dormancy period experiences a substantial increase, reaching 7.8 m.

Notably, the second cyclone dormancy period disappears entirely under SSP5-8.5, suggesting that Bangladesh may face extreme storm-tide hazards during winter—a situation unlikely under the current climate. This shift underscores the need for adaptive strategies to address the growing risk of compounded flooding events under future warming scenarios.

In contrast to severity, seasonal storm-tide frequency changes are not unanimous across scenarios. While there are indications of a potentially many-fold increase in back-to-back flooding events during post-monsoon seasons under the SSP5-8.5 scenario, the frequency remains stable under the SSP2-4.5 and SSP3-7.0 scenarios. Figure 7 illustrates the seasonal frequency shifts based on CMIP6 climate models for storm tides exceeding a 2-m threshold, which we attribute to the combined impact of TC climatology change and SLR. The most significant rise occurs during the post-monsoon season, particularly in October. Table S9 summarizes the projected storm-tide frequency and increased ratios. More frequent events during each period will decrease the interval between occurrences, leading to a higher likelihood of back-to-back coastal flooding.

DISCUSSION

Bangladesh as a country is the most vulnerable in the world to TCs and storm tides, with a history of severe mortality. The lack of accurate storm-tide risk assessments under future climate conditions significantly hampers coastal adaptation, infrastructure planning, and resilience efforts. In this study, we present a comprehensive and precise assessment of storm-tide risks along Bangladesh's entire coastline, considering middle- to high-emission pathways and using a coupled downscaling and hydrodynamic approach. Our findings provide timely and valuable guidance for policymakers in designing effective climate adaptation and resilience strategies. Several key findings from our results merit further discussion.

Comparison with previous studies

Reliably estimating the frequency of extreme storm tides is challenging, particularly in regions with insufficient observations, such as Bangladesh. Even studies evaluating Bangladesh's storm-tide hazard under current climate conditions are limited, let alone those addressing future scenarios. Khan et al.[33] applied the same downscaling-hydrodynamic method to assess storm-tide hazards in coastal Bangladesh but confined their analysis to the current climate. By comparing their results with other existing return-period estimates, they suggest that a biased extreme TC-event sampling strategy in previous studies may overestimate storm-tide return periods. For example, Jakobsen et al.[42] estimate that the 100-year water-level height is about 5 m at the mouth of Meghna and about 8–10 m at Sandwip.

In contrast, Khan et al.'s estimates are about 4 m at the mouth of Meghna and about 6 m at Sandwip. Unsurprisingly, our current climate estimates align with those of Khan et al. We estimate that the 100-year storm tide at these two locations (see estimation

Please cite this article in press as: Qiu et al., From decades to years: Rising seas and cyclones amplify Bangladesh's storm-tide hazards in a warming climate, One Earth (2025), https://doi.org/10.1016/j.oneear.2025.101273

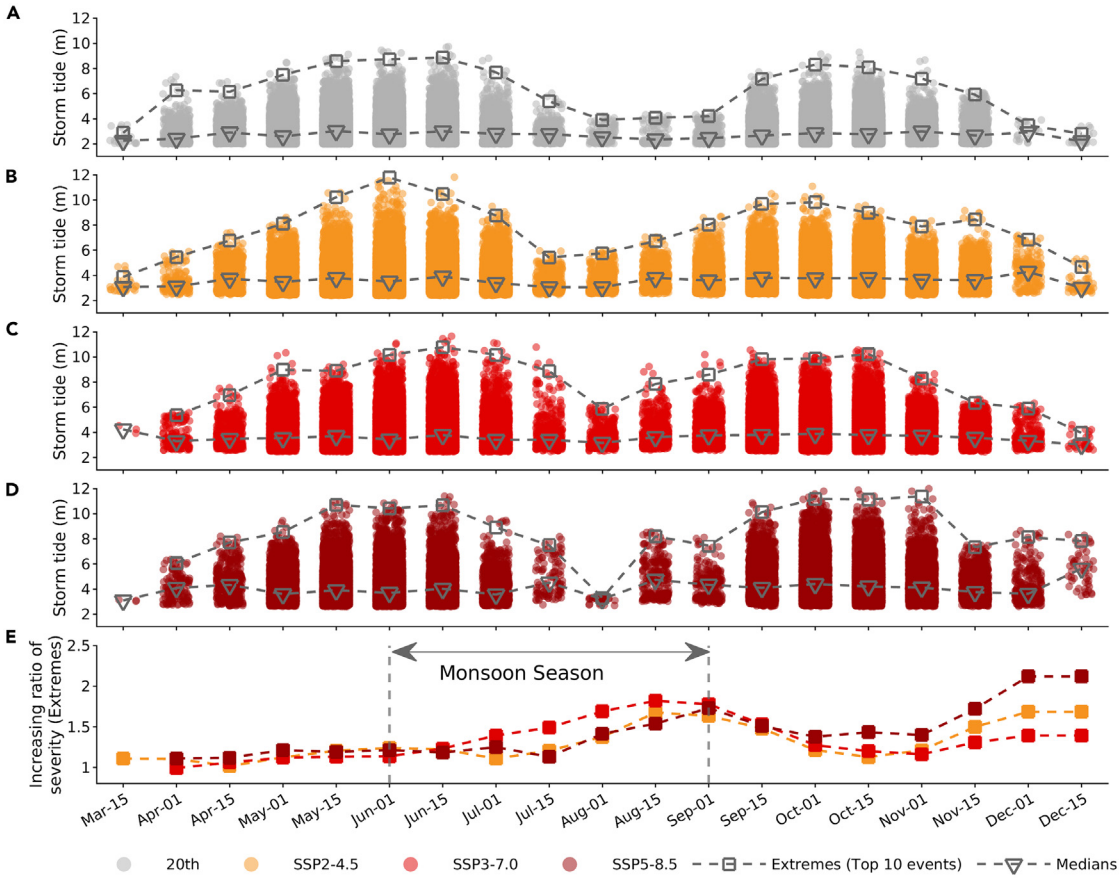

Figure 6. Shifted seasonal regimes of storm-tide severity (greater than 2 m water-level height) based on CMIP6 climate model ensembles

(A–D) Seasonal distribution of storm-tide severity under the current climate and CMIP6 SSP2-4.5, SSP3-7.0, and SSP5-8.5 climate scenarios, respectively. As shown in (A), two relatively inactive storm-tide seasons are identified based on their seasonal behavior under the current climate: one during the late summer monsoon (±7 days around August 1, August 15, and September 1) and the other during the late post-monsoon (±7 days around December 1 and December 15). (E) The increasing ratio of extreme storm-tide intensities across the year, with a 3-point sliding average applied to obtain monthly ratios.

The open square located at the top of each swarm in plots (A), (B), (C), and (D) indicates the mean value of the top ten extremes, while the area between two vertical dashed lines in plot (E) indicates the monsoon season of the BoB.

under the current climate in Figure 3) is about 4.2 m (Meghna region average) and 5.8 m (VS Navi with ID 31), respectively.

Leijnse et al.[28] estimate future climate storm-surge return periods in Bangladesh. Their estimate of the 100-year surge level (without incorporating astronomic tide) for Charchanga and Chittagong is over 60 cm lower than that reported by Khan et al. Several limitations in Leijnse et al.'s methodology may contribute to this discrepancy. Their hydrodynamic model lacked the updated bathymetric data in northern BoB. Further, they apply a purely statistical approach based on the historical TC dataset to generate synthetic TCs without an explicit representation addressing TC activity change under warming climates. As a result, significant uncertainties may remain in their return-period estimation. For this reason, we do not make the comparison here.

Comparison across scales, models, and scenarios

Our projections at regional and local scales reveal a pronounced vulnerability in the Meghna-North Chattogram region despite the widespread distribution of TC tracks across the BoB. Simulations suggest that the funnel-shaped morphology of this region frequently amplifies surges from TCs traveling north and northeast. These storms often move along the coast and reflect off the Chattogram coastline, which runs parallel to the longitude, depositing significant surge energy at the mouth of the Meghna River. Similarly, surges from storms traveling west also follow the Chattogram coastline, culminating in high surge levels in the Meghna-North Chattogram area.

The interplay between the BoB's funnel-shaped morphology and the TC wind-field structure creates a unique and heightened risk for this segment, as highlighted in previous studies.[38] While our assessment provides valuable insights for localized coastal climate adaptation planning and risk mitigation, it is crucial to recognize that the Meghna-North Chattogram region's vulnerability also poses significant risks to the substantial upstream population.

The elevated storm-tide risk under CMIP6 SSP5-8.5 (Figure 3) compared to CMIP5 RCP8.5 (Figure S7) is primarily attributable to the greater frequency and intensity of TCs projected under SSP5-8.5, given the use of identical SLR samples in both RCP8.5 and SSP5-8.5 simulations. Equations 1 and 2

Please cite this article in press as: Qiu et al., From decades to years: Rising seas and cyclones amplify Bangladesh's storm-tide hazards in a warming climate, One Earth (2025), https://doi.org/10.1016/j.oneear.2025.101273

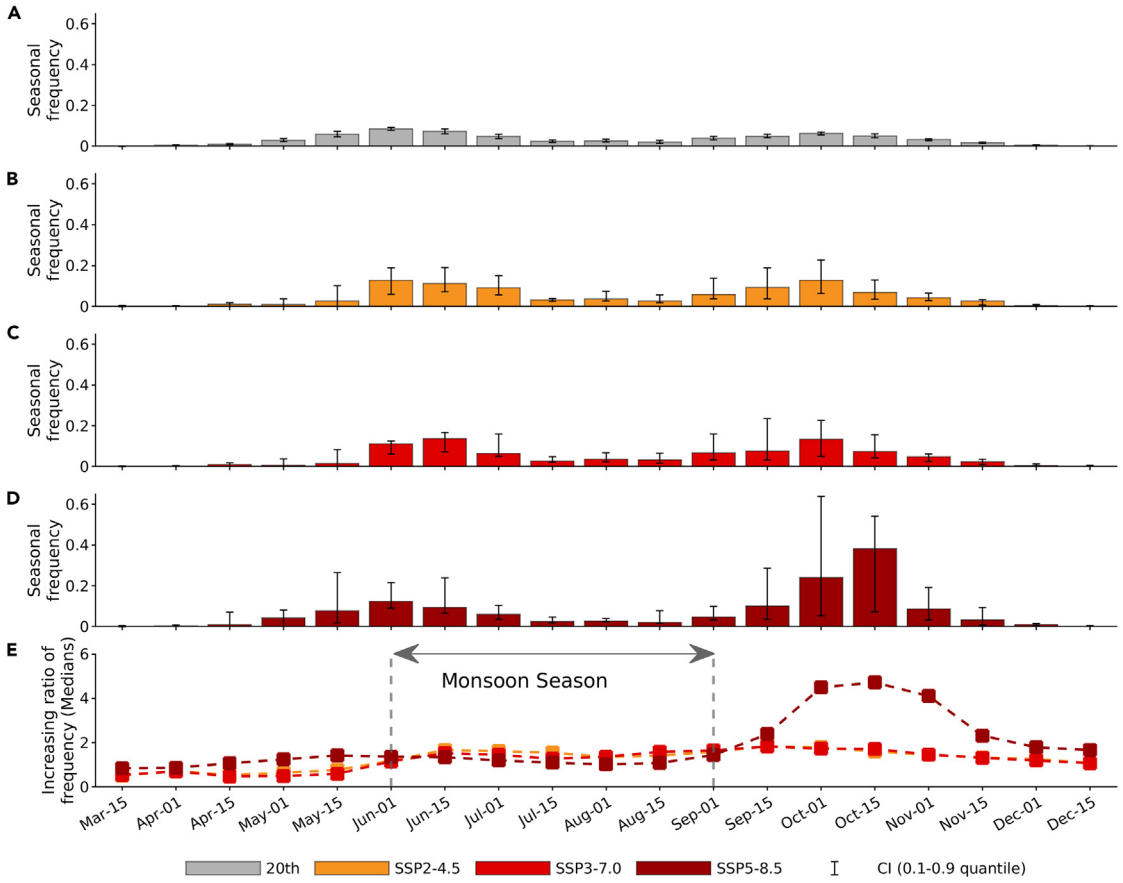

Figure 7. Shifted seasonal regimes of storm-tide frequency (greater than 2 m water-level height) based on CMIP6 climate model ensembles

(A–D) Seasonal distribution of storm-tide frequency under current climate and CMIP6 SSP2-4.5, SSP3-7.0, and SSP5-8.5 climate scenarios, respectively.

(E) The increasing ratio of storm-tide frequency for the medians throughout the year, with a 3-point sliding average applied to get monthly ratios.

The error bars indicate the confidence interval (CI) from the 0.1 to 0.9 quantiles. The area between two vertical dashed lines in plot (E) indicates the monsoon season of the BoB. The CIs account for variability in climate models and multiple-station data.

(see methods) illustrate an inverse relationship between annual TC frequency and storm-tide severity, as captured in the storm tide-exceedance probability curve. Additionally, Figure S26 demonstrates that storm-tide levels and exceedance probabilities are inversely related.

An increase in TC annual frequency for a fixed return period T reduces the return period for the same water level, leading to a higher storm tide associated with that return period. Specifically, as shown in Figure S10, TC frequency under SSP5-8.5 is significantly higher, with a median of 1.7 (CI 0.7–2.5), compared to RCP8.5, which has a median of 0.8 (CI 0.5–1.2).

Furthermore, Emanuel's[7] TC wind projections for Bangladesh indicate that TC wind intensity increases more substantially under SSP5-8.5 than under RCP8.5. The 100-year TC wind intensity rises from 63.2 m/s (123 knots) under the current climate to 75.5 m/s (145 knots) under RCP8.5 and further escalates to 86.4 m/s (168 knots) under SSP5-8.5.

The differences in TC projections between CMIP5 and CMIP6 are partly attributable to the more extensive spread and generally higher average equilibrium climate sensitivity (ECS) within the CMIP6 model ensemble compared to CMIP5.[43,44] The choice of climate model also plays a significant role. For example, even within the same climate model families (e.g., IPSL and MIROC, as shown in Figure S10), TC frequency projections differ substantially between the fifth and sixth generations under both middle-pathway and high-pathway scenarios.

This disparity is likely due to the generally higher ECS values in CMIP6 compared to CMIP5, driven primarily by more substantial positive low-cloud feedback. Previous studies[43,44] emphasize that these feedback mechanisms amplify warming projections, which, in turn, influence TC activity projections under future climate scenarios.

The storm-tide estimates under the SSP2-4.5 and SSP3-7.0 scenarios are similar in magnitude regardless of whether SLR is considered, but remain lower than those projected under the SSP5-8.5 scenario, as shown in Figures 2, 3, and S1–S3. Figure S29 provides an example of storm-tide severity (empirical exceedance probability-storm tide curves) under the EC-Earth3 model at VS Navi without considering SLR.

Under SSP3-7.0, storm-tide severity exceeds that under SSP2-4.5, driven by more intense TCs associated with higher emission pathways. However, the TC annual frequency is lower under SSP3-7.0 compared to SSP2-4.5 (see Figure S10). The combined effects of TC annual frequency and storm-tide severity,

Please cite this article in press as: Qiu et al., From decades to years: Rising seas and cyclones amplify Bangladesh's storm-tide hazards in a warming climate, One Earth (2025), https://doi.org/10.1016/j.oneear.2025.101273

as described by Equations 1 and 2, counterbalance one another, resulting in annual storm-tide levels of comparable magnitude under the SSP2-4.5 and SSP3-7.0 scenarios. Additionally, five out of seven CMIP6 models exhibit a higher TC annual frequency under SSP2-4.5 compared to SSP3-7.0, although the difference in magnitude remains relatively small.

Our observations indicate a higher storm-tide risk (lower median return-period values) for the historical cyclone Bhola under SSP2-4.5 compared to SSP3-7.0, as shown in Figure 5A. Differences in storm-tide return periods and associated dynamics between the two scenarios drive this disparity. Specifically, among the seven CMIP6 models analyzed, two (MRI-ESM2.0 and CanESM5.0.3) exhibit higher return periods under SSP3-7.0 than under SSP2-4.5 for a storm-tide level of 6.1 m at Northern Bhola Island. This leads to a higher median storm-tide return periods under SSP3-7.0 compared to SSP2-4.5.

For illustration, MRI-ESM2.0 is highlighted as a representative example in Figure S30A (results for the other six models are not shown). In contrast, the remaining five models demonstrate similar or lower return periods under SSP3-7.0 compared to SSP2-4.5 for the same storm-tide level. The combination of higher storm-tide severity (see Figure S30B) and greater annual TC frequency under SSP2-4.5 (see Figure S10) results in lower return periods for the same storm-tide level relative to SSP3-7.0. Equations 1 and 2, along with the inverse relationship between storm tides and exceedance probabilities, provide insights into these results.

Limitations and future perspectives

There are a few limitations to this study that require further improvement. First, the hydrodynamic model does not account for wave setup, which refers to the increased water level at the coast caused by the breaking of waves in the surf zone. While wind waves naturally contribute to extreme water levels and are valuable in site-specific applications,[28,34,45] studies in Bangladesh suggest that wind waves typically account for 10%–15% of the maximum total water level.[10,46] Since our primary focus is quantifying large-scale climate change impacts, using storm tides is a practical impact variable. Simulating over 100,000 TCs downscaled from six CMIP5 and seven CMIP6 climate models would possibly add over two orders of magnitude of computational effort to our resources without changing our conclusions. We encourage future studies to explore more computationally efficient approaches for quantifying climate risk while considering the influence of waves, such as representative TC sampling[45] or machine-learning-based wave emulation.[47]

Second, significant uncertainty exists at the nexus of climate scenarios, climate models,[48] and SLR.[49] Although the newer CMIP6 has reduced these uncertainties compared to CMIP5, there is still a need for future research to tighten the scenarios and improve the accuracy of these models in projecting the atmospheric (e.g., cloud feedbacks and cloud-aerosol interactions) and oceanic variables that control TC activity and sea-level dynamics.

Third, it is essential to note that TCs induce storm surges but also produce extreme precipitation, especially when they stall during landfall. Emanuel[7] projects a 20-fold increase in severe storm accumulated rainfall (exceeding 1,000 mm in Dhaka) due to climate change. The potentially growing overlap with the monsoon season and summer heat stress[50] should motivate future research to consider these factors jointly in Bangladesh, integrating coastal (including wave), fluvial, and pluvial process components,[51–53] in addition to the compound effects of TC winds and rainfall that is well under way in the community.

Fourth, in this paper, the monsoon season (June 1 to September 1) is defined based on the present climate and applied as-is in future projections. While our study does not directly focus on the monsoon, it provides a new perspective on potential future monsoon changes in Bangladesh from the perspective of cyclones. We recommend a study of interactions between TC and the monsoon in future studies.

Lastly, this study assumes that bathymetry and morphology will remain unchanged by the end of this century under future climate scenarios. However, bathymetry and morphology will likely evolve over this time horizon, particularly in a dynamic deltaic system shaped by complex sediment transport processes and human disturbances.[54] We recommend that future studies incorporate time-evolving bathymetry and morphology through interdisciplinary collaboration with estuarine geomorphologists to achieve more robust long-term projections.[55,56]

Implications

Our study has broad implications for understanding and mitigating the risks posed by future storm tides. By estimating the return periods of storm tides that account for the combined effects of future TC climatology changes and SLR and analyzing storm-tide distributions across seasons in terms of severity and frequency, our findings provide critical insights. These results can inform policymakers and stakeholders in agriculture, aquaculture, water resources, and urban planning about when and where to prioritize efforts to enhance coastal resilience and mitigate risks, leading to more targeted and practical solutions in a changing climate.

Our analysis underscores the need for future planning, rehabilitation, and improvement of infrastructure investments to focus on the Meghna region and northern Chattogram. Additionally, the growing risks of cascading inland-coastal flooding during the late summer monsoon (August) and back-to-back coastal floods during the post-monsoon period (October and early November) deserve greater attention. Examples of such investments include the World Bank-supported CEIP and Multipurpose Disaster Shelter Project (MDSP).[9] CEIP phase I estimated that the annual risk from cyclone-induced flooding across coastal Bangladesh under the current climate amounts to US$300 million, a figure projected to rise to US$570 million (a 90% increase) under future climate scenarios.[9] These projections assumed a deterministic 0.5-m SLR and an 8% increase in TC wind speeds, which might significantly underestimate the true risks.[34]

Accurately estimating the probabilities of extreme storm tides and their seasonal distributions is urgent. A well-designed risk-mitigation plan can safeguard livelihoods, reduce financial burdens by minimizing disaster impacts, and avoid unnecessary and costly overprotection measures.[57] Furthermore, our storm-tide risk estimates provide critical ocean-side boundary information for hydrologists and engineers. By integrating coastal (including wave), fluvial, and pluvial processes, these findings can help create compound inundation maps for Bangladesh, enabling more comprehensive and effective climate adaptation strategies.

Please cite this article in press as: Qiu et al., From decades to years: Rising seas and cyclones amplify Bangladesh's storm-tide hazards in a warming climate, One Earth (2025), https://doi.org/10.1016/j.oneear.2025.101273

Although our study focuses on Bangladesh, the coupled downscaling and hydrodynamic framework is applicable to other low-lying regions that face similar threats and urgently require tools to improve risk assessments and strengthen resilience planning in a changing climate. Such regions include East Africa (e.g., Mozambique),[13,14] the Philippines,[15,16] Myanmar,[17] Vietnam,[18,19] and southern China.[20–22]

METHODS

Synthetic TC downscaling

We use a statistical-physical downscaling technique to create sets of synthetic TCs that affect Bangladesh.[23,24] The method uses thermodynamic and kinematic statistics from gridded global reanalyses or climate models to produce many synthetic TCs. Initially, we synthetically generate wind time series at 250 hPa and 850 hPa levels as a Fourier series of random phases and a geostrophic turbulence power-law distribution of the kinetic energy spectrum constrained to have accurate monthly means, variances, and covariance. We obtain these statistics and large-scale environmental factors such as potential intensity, wind shear, humidity, and ocean thermal stratification from gridded global reanalyses or climate models.

The time-evolving environment is seeded randomly in space and time with warm-core vortices drawn from a Gaussian distribution of peak wind speeds centered at 12 m/s (25 knots). Seed vortices propagate forward with a weighted average of synthesized winds at the 250 hPa and 850 hPa levels, according to the beta-and-advection model.[58] We then calculate the intensity of the vortices deterministically following the track using the coupled hurricane intensity prediction system (CHIPS) model,[59] which phrases the dynamics in angular momentum coordinates that allow for very high spatial resolution in the storm core. The thermodynamic input to the intensity model includes monthly mean potential intensity, along with 600 hPa temperature and specific humidity, derived from global climate models. The intensity model also accounts for salinity effects on density, affecting TC potential intensity, since the BoB has strong salinity gradients, especially in summer.[7] The storms used here are identical to the ones used in the cyclone study,[7] with additional storms generated to model the SSP2-4.5 and SSP3-7.0 scenarios.

Over 99% of the seeded tracks dissipate quickly and are discarded. The remainder successfully grows to make up the downscaled TC climatology of a reanalysis or climate model. Only seeds that develop a maximum wind speed of at least 21 m/s (40 knots) during their lifetime become synthetic TCs. We represent each simulated synthetic TC as an hourly time series of storm parameters, including time, central position, maximum wind speed, pressure deficit, and radius to maximum wind.

Bangladesh TC catalog

We identify synthetic TCs affecting Bangladesh based on their passage over one or both of the two-line segments displayed in Figure S9. Overall, we generated a total of 100,200 physically consistent TCs. This large catalog amply resolves the tails, significantly reduces extrapolation uncertainties, and enhances the robustness of the risk assessment.

Our catalog includes ECMWF/ERA5 and GMAO/MERRA2 climate reanalyses, yielding 4,100 TCs for the current period (1980–2020), representing 5,860 synthetic years based on the annual TC frequency of 0.7 (see Figure S9). Please see Emanuel et al.[24] for comparisons of downscaled TC behavior with observations across basins, and see Emanuel[7] specifically for Bangladesh.

We also generate 2,000 TCs using six CMIP5 and seven CMIP6 global climate models for two time periods: 1981–2000 for historical simulations; and 2081–2100 for RCP4.5 and RCP8.5 (CMIP5) and SSP2-4.5, SSP3-7.0, and SSP5-8.5 (CMIP6) simulations. We select the climate models based on the availability of climate variables and in alignment with the previous study.[7] Table S2 summarizes additional information about this study's reanalyses and climate models.

Hydrodynamic simulation of storm tide

We used ADCIRC (Advanced Circulation model, two-dimensional barotropic tides, version 56.02)[35,60,61] for storm-tide simulations. Preparing this model requires several steps—mesh generation, model configuration, and model verification—as discussed in this section.

Mesh generation

We use OceanMesh2D[62,63] to generate a varying-resolution unstructured mesh for BoB (spanning latitudes from 9°N to 23°N and longitudes from 80°E to 100°E). OceanMesh2D generates a mesh based on several feature-driven geometric and topographic-bathymetric mesh size functions, providing adequate resolution to capture the intricate coastal characteristics. The final unstructured mesh consisted of 42,915 vertices and 77,385 triangular elements, with a resolution ranging from 20 km over the deep ocean to 250 m near the coastlines (see Figure S11). Table S4 summarizes the mesh size functions and their corresponding parameters for spatially distributed resolution.

Bathymetry and shoreline. To represent bathymetry and shorelines in the computational mesh, we used data from different sources for the primary BoB and the Bengal Delta.

For the primary BoB, the full-resolution Global Self-consistent Hierarchical High-resolution Shorelines (GSHHS, version 2.3.7, the vertical datum is mean high water) dataset[64] defines the shoreline boundaries, and the General Bathymetric Chart of the Oceans (GEBCO, version 2024, the vertical datum is mean sea level) on a 15 arc-seconds geographic latitude and longitude grid[65] is the source of bathymetry data.

For the Bengal Delta, we utilize higher-resolution shoreline and bathymetry data. We derive the shoreline boundaries from the vectorized OpenStreetMap water layers (version2),[66] while an updated bathymetric dataset[33,36] provides the bathymetry, which incorporates 77,000 newly digitized points from 34 updated Bangladesh navigational charts (see previous studies' supplementary material[33,36]). We interpolate the bathymetric measurement points for the Bengal Delta (originally referenced to chart datum and subsequently unified to mean sea level) onto a structured grid with a 200-m resolution to generate the digital elevation model (DEM) using a simple kriging method.[20] Bathymetry and bathymetric slope were interpolated onto inner (Bengal Delta) and outer (BoB) mesh vertices directly from the original DEM, then merged to ensure consistency across the connected areas (see Figure S12). The function *lim_bathy_slope* in OceanMesh2D kept the maximum bathymetric gradient below 0.1, which is essential to ensure numerical stability.[62] The constraint helps maintain the water-depth variation

Please cite this article in press as: Qiu et al., From decades to years: Rising seas and cyclones amplify Bangladesh's storm-tide hazards in a warming climate, One Earth (2025), https://doi.org/10.1016/j.oneear.2025.101273

between adjacent nodes within a defined slope, minimizing unrealistic or abrupt changes in the model.

Mesh boundaries. The mesh's outer node string boundary includes both oceanic and riverine boundaries. We classify segments as the mainland boundary if their distance from the shoreline is within 0.4 geographic degrees and their depth relative to sea level is less than 30 m. In contrast, the remaining segments become ocean boundaries. To account for the impact of upstream riverine flow, we implemented 29 normal flux boundaries within the mesh. The locations of river inflows were identified based on the availability of bathymetric data and the attributes of vectorized river reaches, such as average discharge, bankfull discharge, average river width, and length.[67] Details regarding the setup of riverine flow in OceanMesh2D are available in a previous study,[20] and Figure S13 illustrates the final mesh boundary conditions.

Model configuration

The model setup involves configuring the inputs, forcings, and parameters, as discussed next.

Upstream riverine input. Accurate upstream riverine discharge inputs are challenging in the complex deltaic model because long-term reliable observations for the Bengal Delta river network are lacking. A common approach is to assume an average climatological upstream discharge for astronomical tide and cyclone-induced storm-tide periods, providing a constant hourly input to drive the model at the upstream boundary.[33,68] The global reach-level estimation supplied in a previous study[67] provides climatological discharge data in our study. We note that sensitivity experiments (driving the model with ten discharge values ranging from the average discharge and bankfull discharge) demonstrate that both the astronomical tide and storm-tide model responses are not sensitive to the upstream discharge forcing, as the locations of our tidal stations (and VSs) are far from regions influenced by riverine dynamics. The same assumption also applies to the synthetic TC simulations.

Meteorological forcing. We use the analytical wind profile model derived by Chavas et al. (CLE15)[69] to calculate the 1-min average storm wind at the gradient level. CLE15 is a physics-based model that integrates two existing TC theories to represent wind variations in the inner and outer core regions.[70,71] These two solutions are seamlessly connected at a merging point, ensuring the mathematical continuity of both the angular momentum and its radial derivative. CLE15 utilizes the maximum wind speed and the radius of maximum wind to compute the complete wind profile. To account for the asymmetry of the wind field, we apply the asymmetrical wind model developed by Lin and Chavas (LC12)[72] to add surface environmental wind to the storm wind. The gradient wind is converted to the 10-m winds using a surface wind reduction factor (SWRF) of 0.8 (calibrated) and an empirical formula for inflow angles.[73] A reduction factor of 0.893 converts the 1-min average wind to a 10-min average[74] for the simulations.

The parametric pressure model[75] calculates the radial pressure profile based on the pressure deficit. The Powell formulation,[76] with a capped wind drag coefficient (C_d) of 0.0016 (calibrated), converts surface wind velocity into wind stress. A previous study demonstrated that the CLE15-LC12 coupling wind model provides a superior method for simulating TC-induced storm tides compared to the traditional Holland1980 wind model[75] with its translation-speed-based asymmetric approach.[77] Our testing experiments also indicate that the Holland1980 wind model tends to underestimate storm surges, whereas the CLE15 wind model performs more accurately, consistent with the conclusions of Wang et al.[77]

Astronomical tide forcing. We take 15 astronomical tidal components into account to obtain more precise and comprehensive astronomical tide solutions, including eight major tides (M_2, S_2, N_2, K_2, K_1, O_1, P_1, and Q_1), two long-period tides (*Mf* and *Mm*), three nonlinear tides (M_4,MS_4,and MN_4), and two minor tides ($2N_2$ and S_1). The self-attraction, loading (SAL), and internal tide terms are also considered.[78,79] The latest global satellite-assimilated tidal model TPXO10-Atlas-V2 with a resolution of 1/30°[80] provides the equilibrium tide for the model domain and the periodic tidal signals along the oceanic open boundaries. We interpolate the amplitudes and phases of the SAL terms from FES2014 data-assimilated tidal solutions.[81] The internal tide drag coefficient (C_{it}) is set to 2.2, with a depth cutoff of 100 m, based on globally optimized results for the Indian Ocean.[82]

Bottom friction. Boundary layer dissipation in nearshore shallow areas primarily influences tidal solution accuracy. Manning's *N* parameterizes quadratic bottom friction, whose depth dependency enables better redistribution of resistance. Here, we follow an approach similar to that of previous studies[10,33,36] but with further optimization for the spatial distribution to ensure consistency between simulations and observed tidal signals. Figure S14 illustrates the spatially optimized Manning's *N* coefficient.

For water depths greater than 20 m, we set the Manning's *N* coefficient to 0.02. In the Bengal Delta, where water depths are less than 20 m, we initially divide the region into five subdomains (each with a tidal gauge station) for parameter optimization. After conducting a series of sensitivity tests, we determined that using a Manning's *N* coefficient of 0.013 for the left three regions (covering the Sargar Road, Hiron Point, and Dhulasar stations) and 0.01 for the right two regions (covering the Chachanga and Chittagong stations) ensures that the tidal solutions at the five stations achieve an accuracy comparable to and consistent with that reported in previous studies.[10,33,36]

The lower bottom friction identified in the Meghna-Chattogram coastal plain is likely attributable to its fine-grained silty substrate.[83] Pringle et al.[84] report a similar phenomenon in the Yellow Sea region of China. We recommend additional optimization of bottom friction dissipation using semi-data-informed approaches[84] when detailed and accurate sediment type information becomes available for the nearshore Bengal Delta.

Computational performance. To balance computational cost and ensure numerical stability for ensemble simulations, selecting an appropriate time step and domain decomposition strategy (CPU cores used for parallel simulation) is crucial. Based on previous experience,[61] we determined a maximum time step of 40 s for the 250-m mesh. Using cyclone Sidr (2007), we tested the impact of domain decomposition on simulation wall-clock cost. We found that a parallel strategy with approximately 40 domains maximized computational efficiency, with limited gains observed beyond this point, providing critical insights into optimal computational resource allocation. Figures S15 and S16 display the mesh decomposition and efficiency performance, respectively. Besides, the 40-s time step proved robust for synthetic TC-storm-tide simulations, with only a tiny fraction

Please cite this article in press as: Qiu et al., From decades to years: Rising seas and cyclones amplify Bangladesh's storm-tide hazards in a warming climate, One Earth (2025), https://doi.org/10.1016/j.oneear.2025.101273

(approximately 0.5%) crashing. A reduced time step of 10 s corrected all the failed simulations without affecting the others. We apply a 2-day model spin-up to all simulations.

Model verification

Accurate simulation of astronomical tides is essential for reliably modeling storm tides. In this section, we verify astronomical and storm-tide performance, collecting substantial data.

Astronomical tide verification. We compare the model's output with harmonic constituents at five tide gauge stations Sagar Roads, Hiron Point, Dhulasar, Charchanga, and Chittagong (see Figure 1 and Table S1 for detailed locations). The model was initially driven by five leading astronomical tidal constituents (M_2, S_2, N_2, K_1, and O_1) for 30 days, with 2 days for spin-up and 28 days for harmonic analysis.[61,85] The co-tidal chart (see Figure S17) illustrates tidal wave propagation patterns, which aligns with the findings of previous studies.[86,87] The spatially distributed root-mean-square error (RMSE) discrepancies for each tidal constituent compared to the TPXO-10-Atlas-V2 are less than 2.5 cm across most of the ocean (Figure S18), indicating that our model performs well in the primary BoB basin.

However, we note relatively higher discrepancies at the head of the Bengal Delta. This is primarily due to the model grid of TPXO-10-Atlas-V2 not extending into the river network and the lack of assimilation of accurate bathymetric data in these nearshore areas. Thus, the TPXO-10-Atlas-V2 product itself exhibits significant uncertainty in these shallow areas. By employing spatially optimized Manning's N coefficient in the Bengal Delta, the total complex error of all four available constituents (M_2, S_2, K_1, and O_1) is comparable to that of previous studies,[10,33,36] the global satellite, and site-assimilated TPXO-10-Atlas-V2 model, as shown in Table S5.

Storm-tide data collection and processing. Accurately simulating storm tide requires high-quality water-level measurements for model verification. The lack of water-level observations during TC landfalls in Bangladesh poses a significant challenge. To address this, we assembled the most comprehensive water-level observations available to date for storm-tide verification. We collected long-term water-level observations from two tidal stations, Hiron Point (sourced from Bangladesh Inland Water Transport Authority [BIWTA]) and Chittagong (sourced from the University of Hawaii Sea Level Center [UHSLC]), starting in 2007. We also collected water-level observations from two other stations, Khepupara and Cox's Bazaar (sourced from BIWTA), during cyclone Sidr's (2007) landfall. Since the Khepupara station stopped working after Sidr's landfall, we obtained an estimate of the peak water level from the ITJSCE report.[88,89]

Consequently, our dataset includes water-level observations from eight recent TCs that made landfall in Bangladesh or India but significantly impacted Bangladesh. For four of these TCs, verification data from two stations were available. In contrast, for Sidr, data from four stations were available, with stations distributed on both sides of the TC's forward path. Thus, we assembled the most comprehensive water-level observations for model verification.

Some processing was further required to use the observations effectively. The observations were based initially on local chart datum and Bangladesh standard time (UTC + 06:00). To ensure consistency in model verification, we converted them to local mean sea level and UTC. The datum conversion used were Hiron Point (−1.86 m), Chittagong (−3.50 m), Khepupara (−2.30 m), and Cox's Bazaar (−2.10 m), averaged over multiple years of observations. Previous studies[38,89] report similar datum-conversion values, and UHSLC's official website also documents datum information for several stations.

Storm-tide verification. Having processed the observational data, we use statistical metrics from multiple historical TCs at various stations to evaluate the model's performance in simulating storm tides. As shown in Figure S19, the overall RMSE of 0.25 m with a 0.94 coefficient of determination (R^2) indicates that our model performed well in simulating peak storm tides. In addition, Figure S20 shows strong agreement in both storm-tide phase and amplitude for cyclone Sidr (which was the only cyclone for which observations at many stations were available). For visualization, Figure S21 also displays Sidr's peak storm-tide map. Thus, the hydrodynamic model's storm-tide simulation performance is consistent with other results and reasonably verified.

IPCC AR6 relative sea-level projection

Our probabilistic, localized relative sea-level projections are based on the Framework for Assessing Changes to Sea-level (FACTS),[90] which emphasizes the role of the Antarctic and Greenland ice sheet as drivers of structural uncertainty in sea-level rise projections. FACTS can generate seven alternative probability distributions relative to a 1995–2014 baseline under multiple alternative emission scenarios presented in the Intergovernmental Panel on Climate Change Sixth Assessment Report (IPCC AR6).[49]

In this study, we apply the gauge-based Monte Carlo samples[90] (20,000 in total) of future relative sea level under workflows 2-E and scenarios CMIP6 SSP2-4.5 (Figure S22), SSP3-7.0 (Figure S23), and SSP5-8.5 (Figure S24), covering the period from 2080 to 2100. The workflow 2-E of FACTS employs Gaussian process emulation for Greenland, glaciers, and Antarctica and forms the basis of the "medium confidence" projections presented by IPCC AR6. The four gauge-based stations located in coastal Bangladesh are Hiron Point (permanent service for mean sea level [PSMSL] ID 1451), Khepupara (PSMSL ID 1454), Charchanga (PSMSL ID 1496), and Cox's Bazaar (PSMSL ID 1476). We assume that the sea level will rise monotonically within each decade. Thus, we represent the distributions using statistics at 2080, 2090, and 2100, linearly interpolated to the year of the simulated storm to get SLR samples. From a sampling perspective, we can thus draw SLR samples, with replacement, from a distribution for any scenario, location, and year of interest, which is essential to incorporate SLR (see section "storm-tide catalog: jointly sampling TCs, tides, and SLR."

Nonlinear interactions

Rising sea levels increase regional water depth, causing the quadratic bottom stress to redistribute with depth. In turn, the total water level driven by both astronomical and meteorological forcing is affected. As shown in Figure S25, neglecting the SLR-surge interaction underestimates the total water level. In our work, we account for the nonlinear interactions among sea level, tides, and storm surges, offsetting the initial sea surface with an SLR sample value paired with each TC sample. The section "storm-tide catalog: jointly sampling TCs, tides, and SLR" provides details on the joint sampling, and "return-period estimation" provides details on the impacts of including SLR.

Please cite this article in press as: Qiu et al., From decades to years: Rising seas and cyclones amplify Bangladesh's storm-tide hazards in a warming climate, One Earth (2025), https://doi.org/10.1016/j.oneear.2025.101273

Storm-tide catalog: Jointly sampling TCs, tides, and SLR

We use a sampling approach to integrate tides and SLR with TCs in storm-tide simulations. A critical feature of this approach is the time association of synthetic downscaled TC samples under specific climate models and scenarios, which connects these three components. The method utilizes the TC's origin and arrival times to synchronize tidal phases and constrain SLR samples to the associated year. By generating an extensive ensemble of synthetic TCs (100 per year) with random times distributed across the decades of interest, the approach effectively produces Monte Carlo samples from the joint distribution of TCs (for a given climate model, scenario, and period), tidal phases, and SLR (varying over the period, sampled from the gauge-based station nearest to the TC landfall location among the four available stations).

This results in an ensemble representing the marginal distribution of storm tides that incorporates the complex interactions between these effects. For a large ensemble, this strategy offers several advantages. First, linking TC timing with tides and SLR avoids relying on an oversimplified linear relationship between these variables. Additionally, it enhances scalability by circumventing the combinatorial explosion that would result from explicitly rotating the tidal phase for each storm or pairing every SLR sample with each TC.

Synchronizing storm timing with the tide implicitly accounts for tidal phase effects. For SLR, previous studies have used convolutional methods[91] or copula-based approaches[92] to derive the cumulative distribution function of storm tides. However, these methods face significant limitations. Copulas are particularly challenging to construct, especially in scenarios involving complex dependencies and nonlinearities. Convolution, by definition, assumes linearity and shift invariance and is applicable only when the distributions are independent. This assumption does not hold for the nonlinear interactions between TCs, tides, and SLR, as tides and SLR are also influenced by the properties of TC events.

Monte Carlo sampling overcomes these challenges by accommodating nonlinear dependencies. In cases where the relationships are linear and independent, it is easy to see that Monte Carlo converges to the convolutional case in the large sample limit. However, it remains the only generally viable method for capturing nonlinear interactions among tides, SLR, and TCs. TC characteristics influence SLR, and tides and are not independent variables.

To be sure, hydrodynamic simulations do not inherit a single SLR (or a few) values representing the entire time interval (e.g., 2081–2100). The SLR distributions, which change with the year (see Figures S22–S24), are sampled to randomly associate with TCs generated in that year (100 pairs). We posit that this is reasonable (given typical annual TC frequencies) for sampling SLR.

Statistical analysis

Return-period estimation

The primary statistical analysis produces return periods corresponding to return levels with and without SLR. Further, we separately calculate the storm-tide versus return-period curves for each of the 58 coastal stations. For each storm-tide simulation, we record the highest water elevation during the cyclone's lifetime and the corresponding time. The peak storm tide arrival times help assess the seasonal distribution of extreme storm tides (see the section "shifting seasonal severity and frequency regimes"). The return-period calculations use a vector of 2,000 peaks (per climate model) or 4,100 peaks (for climate reanalyses) and employ the following steps.

We assume that TCs arrive as a stationary Poisson process in a given climate.[93] The storm tide return period, incorporating storm surge and astronomical tide excluding SLR, exceeding a given return level h, uses the formula[91]:

$$T_{\eta_{\text{storm tide(noSLR)}}}(h) = \frac{1}{\lambda \times EP\{\eta_{\text{storm tide(noSLR)}} > h\}}, \quad \text{(Equation 1)}$$

where λ is the TC annual frequency, $EP\{\eta_{\text{storm tide(noSLR)}} > h\} = 1 - P\{\eta_{\text{storm tide(noSLR)}} \leq h\}$ is the exceedance probability of maximum TC-induced storm tide, and $P\{\eta_{\text{storm tide(noSLR)}} \leq h\}$ is the cumulative distribution function. Please note that for climate models and reanalyses, λ, the TC annual frequency, relates to the ratio of successful to unsuccessful seeds in a given year (see the section "synthetic TC downscaling"), with a constant of proportionality established by comparing time averages to dependable historical records. For reference, Bangladesh's historical record suggests $\lambda = 0.7$ (see the section "bias correction") under a Poisson arrival model.

The storm tide return period (incorporating storm surge, astronomical tide, and SLR) exceeding a given return level h uses the same method[91]:

$$T_{\eta_{\text{storm tide(withSLR)}}}(h) = \frac{1}{\lambda \times EP\{\eta_{\text{storm tide(withSLR)}} > h\}}, \quad \text{(Equation 2)}$$

where $EP\{\eta_{\text{storm tide(withSLR)}} > h\} = 1 - P\{\eta_{\text{storm tide(withSLR)}} \leq h\}$ is the exceedance probability (tail probability) of maximum storm tide denoted, and $P\{\eta_{\text{storm tide(withSLR)}} \leq h\}$ is the cumulative distribution function.

Extreme value theory suggests using the generalized Pareto distribution (GPD) to model the upper tail[94] to estimate the storm-tide probability. We fit GPD to the upper tail and a kernel density estimate[95] to the remaining portion (function *paretotails* in MATLAB), as shown in Figure S26. For a given return period, the inverse cumulative distribution function (function *icdf* in MATLAB) calculates the corresponding return levels. We characterize the upper tail as the 98th percentile through a trial-and-error approach, testing from the 95th to the 99th percentile and to ensure the tail achieved the best fit with the smallest RMSE.[91]

These methods apply to each climate model in each scenario and at each station. We estimate the return periods with and without SLR in all scenarios after additionally correcting for bias (see the section "bias correction") and quantifying uncertainty (see the section "storm-tide return period confidence intervals").

Additionally, the section "SLR and TC contributions to storm tides" uses these methods to assess the relative impacts of TC climatology change and SLR on storm tides in future climate scenarios over the interval 2081–2100, relative to the present (1981–2000), each representing a stationary climate regime within which SLR continuously varies (see the section "IPCC AR6 relative sea-level projection"). The section "the future risk of historically deadliest storms" assesses annual frequencies (the inverse of the return period) of historically destructive cyclones using return periods in different climate regimes, including the current climate (which offers better resolution than the observational record) and various warming scenarios.

Please cite this article in press as: Qiu et al., From decades to years: Rising seas and cyclones amplify Bangladesh's storm-tide hazards in a warming climate, One Earth (2025), https://doi.org/10.1016/j.oneear.2025.101273

Bias correction

Climate model projections are biased in various ways, including TC frequency, seasonal distributions, and storm-tide return periods. These biases originate from distinct sources and require tailored correction methods, which we detail below.

TC frequency. As shown in Figure S10, the annual frequency of TCs varies significantly depending on the climate model used. The observed annual frequency of historical TCs (with peak wind speeds exceeding 17 m/s [33 knots]) making landfall in Bangladesh is 0.7, based on 26 events recorded in the JTWC dataset from 1980 to 2020.[96] We assume that TC occurrences follow a Poisson process, making the arrival rate $\lambda = 0.7$ a reasonable representation of the current climate's annual TC frequency. Additional details on landfall events and Poisson distribution fits are provided in Figure S9.

The observed annual frequency calibrates both reanalysis and climate model frequencies. Under the current climate, this calibration entails multiplying the projected annual frequencies in future climate scenarios with a correction ratio derived from the current climate. Table S3 presents the bias-corrected TC annual frequencies for future scenarios. The substantial variation among climate models reflects both systematic differences among models and the inherent uncertainties caused by internal climate variability.[97]

Storm-tide return period. In addition to frequency, biases in storm tide return-period curves are evident (see the section "return period estimation"). We estimate climate model return-level corrections for return periods ranging from 10 to 1,000 years, estimated under the current climate, using Equations 1 and 2. In relation to quantile-quantile mapping,[91,98,99] the fundamental difference is that this uses the estimated return levels at high return periods rather than the underlying samples themselves, and thus are applicable as first-order corrections in future climate simulations. Climate model return levels are adjusted to match the average return levels derived from reanalyses (ECMWF/ERA5 and GMAO/MERRA2) across all return periods in yearly increments. Bias corrections are computed for each station, return period, and climate model in the current climate and applied to the corresponding model, station, and return period for future scenarios. As illustrated in Figure S27, this approach ensures that the entire storm tide return-period curve is effectively corrected, providing consistency and reliability in the assessment of future storm tide risks.

Storm-tide seasonal regimes

Time-indexed synthetic TCs enable the association of arrival times with peak storm tides. For seasonal assessments, we bin bias-corrected storm tides into 14-day windows, defined as ±7 days around the beginning and midpoint of each month. This results in a 24-bin distribution of fractional allocations of annual storm-tide frequencies.

To address seasonal biases, we align the 24-bin distribution between the climate model projections and averaged reanalyses using a methodology similar to the one applied in previous bias corrections. This alignment yields a seasonal storm-tide bias correction for each climate model. The per-model bias correction then applies to future seasonal frequency assessments for the corresponding models.

This seasonal bias correction allows for a detailed evaluation of shifts in storm-tide severity and frequency across different seasonal periods, as further discussed in the section "shifting seasonal severity and frequency regimes."

Storm-tide return period confidence intervals

Within any climate scenario, certain factors reduce the confidence in storm-tide return-period estimates. While the joint sampling of SLR, tides, and TCs (see the section "storm-tide catalog: jointly sampling TCs, tides, and SLR") propagates essential uncertainties (see "limitations of the study" for additional discussion) into storm tides, additional sources remain. We account for two primary sources.

Model error. Climate model ensembles implicitly represent model error, a significant source of uncertainty. The rapid TC downscaling process allows us to account for model error more comprehensively by incorporating a more extensive set of climate models rather than relying on just a few selected models.

Parameter uncertainty in GPD fitting. The fitting procedure for GPDs introduces parameter uncertainties. These uncertainties are quantified using a bootstrap approach, generating confidence intervals from 1,000 trials with replacement. Figure S26 illustrates these bootstrap-derived confidence intervals from the piecewise kernel-GPD fitting process. While GPD-induced uncertainty contributes to confidence loss, it is relatively minor compared to the more substantial impact of model error (see Figure S28).

We assess confidence intervals for storm-tide return periods across all spatial scales (station, regional, national) and climate scenarios. To achieve this, we generate multiple bootstrap samples to fit storm-tide return-period curves for each climate model. We then accumulate the fully mixed ensemble, accounting for both GPD parameter variability and climate model variability. This approach allows us to calculate the mean (or median) return-period curve and its upper and lower confidence bounds, providing a comprehensive assessment of return-period uncertainty for each scenario.

RESOURCE AVAILABILITY

Lead contact

Requests for further information and resources should be directed to and will be fulfilled by the lead contact, Jiangchao Qiu (qiujch24@mit.edu).

Materials availability

Our storm-tide estimates (return-period versus return-level curves) incorporating SLR based on the IPCC AR6 multimodel ensemble are publicly available at https://zenodo.org/records/14982753.

Data and code availability

Some public datasets used for this study are available at https://www.soest.hawaii.edu/pwessel/gshhg/ (GSHHS), http://hydro.iis.u-tokyo.ac.jp/~yamadai/OSM_water/ (rasterized OSM water layer map), https://www.gebco.net/data_and_products/gridded_bathymetry_data/ (GEBCO), https://www.metoc.navy.mil/jtwc/jtwc.html?north-indian-ocean (JTWC), https://www.tpxo.net/global/tpxo10-atlas (TPXO10-Atlas-V2), ftp://ftp.legos.obs-mip.fr/pub/FES2012-project/data/LSA/FES2014/ (FES2014 tidal database), https://github.com/rutgers-ESSP/ipCC-AR6-Sea-Level-Projections (IPCC AR6 sea-level projections), https://uhslc.soest.hawaii.edu/stations/?stn=124#levels (UHSLC tidal data), https://zenodo.org/records/3552776 (global reach-level hydrological attributes). WindRiskTech performs TC-induced risk assessments for clients worldwide and provides datasets free of charge for scientific research upon request (info@windrisktech.com), subject to a non-redistribution agreement.

The hydrodynamic model used in this study is ADCIRC (version 56.02), which can be accessed freely at https://github.com/adcirc/adcirc. The OceanMesh2D toolbox generates the unstructured mesh. It is accessible at https://github.com/CHLNDDEV/OceanMesh2D. MATLAB (version 2022a) *paretotails* function at https://www.mathworks.com/help/stats/paretotails.html provides the piecewise kernel-generalized Pareto distribution fitting. pyTMD, available at https://github.com/tsutterley/pyTMD, provides astronomical tide preprocessing analyses. The codes used to create the unstructured mesh, ADCIRC inputs, and visualization are available from the corresponding authors upon reasonable request.

ACKNOWLEDGMENTS

We acknowledge funding from the MIT Climate Resilience Early Warning Systems Climate Grand Challenges project, the Jameel Observatory JO-CREWSNet project, and the MIT Weather and Climate Extremes Climate Grand Challenges project. Schmidt Sciences provided support. The authors thank Yann Krien for offering the initial improved bathymetric dataset for the Northern Bay of Bengal and A.K.M. Saiful Islam for sharing the updated bathymetric dataset for the Bengal Delta as well as the long-term water-level observations from multiple BIWTA gauge stations. We thank Michael Steckler for sharing the GPS coordinates and observed water-level data for Hiron Point and Khepupara. We thank Md Wasif E Elahi for providing their model output for comparison. We thank Shuai Wang and Coleman P. Blakely for incorporating the CLE15-LC12 wind model into ADCIRC. We also express our gratitude to the developers of ADCIRC and OceanMesh2D, with special thanks to William J. Pringle and Keith J. Roberts for their help over the years. We thank Svetlana Erofeeva for discussing tidal solutions and sharing the latest TPXO10-Atlas-V2 dataset. Last, but not least, we sincerely appreciate the editorial team and three anonymous reviewers for their precious time and valuable suggestions, which have immensely improved the manuscript.

AUTHOR CONTRIBUTIONS

Conceptualization, J.Q., S.R., and K.E.; methodology, J.Q., S.R., and K.E.; investigation, J.Q. and S.R.; verification, J.Q.; visualization, J.Q.; writing – original draft, J.Q. and S.R.; writing – review & editing, S.R. and K.E.; resources, S.R.; supervision, S.R.; funding acquisition, S.R. and K.E.

DECLARATION OF INTERESTS

The authors declare no competing interests.

SUPPLEMENTAL INFORMATION

Supplemental information can be found online at https://doi.org/10.1016/j.oneear.2025.101273.

Received: March 21, 2024
Revised: January 9, 2025
Accepted: March 19, 2025
Published: April 11, 2025

REFERENCES

1. Needham, H.F., Keim, B.D., and Sathiaraj, D. (2015). A review of tropical cyclone-generated storm surges: Global data sources, observations, and impacts. Rev. Geophys. *53*, 545–591.
2. Chowdhury, K. (2002). Cyclone preparedness and management in bangladesh. Improvement of early warning system and responses in Bangladesh towards total disaster risk management approach *115*, 119.
3. Paul, B.K. (2009). Why relatively fewer people died? the case of Bangladesh's cyclone Sidr. Nat. Hazards *50*, 289–304.
4. Islam, T., and Peterson, R.E. (2009). Climatology of landfalling tropical cyclones in Bangladesh 1877–2003. Nat. Hazards *48*, 115–135.
5. Dasgupta, S., Huq, M., Khan, Z.H., Ahmed, M.M.Z., Mukherjee, N., Khan, M., and Pandey, K.D. (2010). Vulnerability of Bangladesh to cyclones in a changing climate: Potential damages and adaptation cost. https://hdl.handle.net/10986/3767.
6. Streatfield, P.K., and Karar, Z.A. (2008). Population challenges for Bangladesh in the coming decades. J. Health Popul. Nutr. *26*, 261–272.
7. Emanuel, K. (2021). Tropical cyclone risk in Bangladesh*72*, pp. 27–34. URL:. https://doi.org/10.54302/mausam.v72i1.122 http://103.215.208.102/index.php/MAUSAM/article/view/122
8. World's deadliest tropical cyclone was 50 years ago. URL: https://wmo.int/media/news/worlds-deadliest-tropical-cyclone-was-50-years-ago.
9. Kazi, S., Urrutia, I., Van Ledden, M., Laboyrie, J.H., Verschuur, J., Haque Khan, Z.u., Jongejan, R., Lendering, K., and Mancheño, A.G.. (2022). Bangladesh: Enhancing Coastal Resilience in a Changing Climate. World Bank. https://hdl.handle.net/10986/38004.
10. Khan, M.J.U., Durand, F., Bertin, X., Testut, L., Krien, Y., Islam, A.K.M.S., Pezerat, M., and Hossain, S. (2021). Towards an efficient storm surge and inundation forecasting system over the Bengal Delta: chasing the supercyclone amphan. Nat. Hazards Earth Syst. Sci. *21*, 2523–2541.
11. Becker, M., Papa, F., Karpytchev, M., Delebecque, C., Krien, Y., Khan, J.U., Ballu, V., Durand, F., Le Cozannet, G., Islam, A.K.M.S., et al. (2020). Water level changes, subsidence, and sea level rise in the Ganges–Brahmaputra–Meghna delta. Proc. Natl. Acad. Sci. USA *117*, 1867–1876.
12. Chen, J., and Mueller, V. (2018). Coastal climate change, soil salinity and human migration in bangladesh. Nat. Clim. Change *8*, 981–985.
13. Tzachor, A., Richards, C.E., Gudoshava, M., Nying'uro, P., Misiani, H., Ongoma, J.G., Yair, Y., Mulugetta, Y., and Gaye, A.T. (2023). How to reduce Africa's undue exposure to climate risks. Nature *620*, 488–491.
14. Nederhoff, K., van Ormondt, M., Veeramony, J., van Dongeren, A., Antolínez, J.A.Á., Leijnse, T., and Roelvink, D. (2024). Accounting for uncertainties in forecasting tropical-cyclone-induced compound flooding. Geosci. Model Dev. (GMD) *17*, 1789–1811.
15. Mori, N., Kato, M., Kim, S., Mase, H., Shibutani, Y., Takemi, T., Tsuboki, K., and Yasuda, T. (2014). Local amplification of storm surge by super typhoon Haiyan in Leyte gulf. Geophys. Res. Lett. *41*, 5106–5113.
16. Lagmay, A.M.F., Agaton, R.P., Bahala, M.A.C., Briones, J.B.L.T., Cabacaba, K.M.C., Caro, C.V.C., Dasallas, L.L., Gonzalo, L.A.L., Ladiero, C.N., Lapidez, J.P., et al. (2015). Devastating storm surges of typhoon Haiyan. Int. J. Disaster Risk Reduct. *11*, 1–12.
17. Fritz, H.M., Blount, C.D., Thwin, S., Thu, M.K., and Chan, N. (2009). Cyclone nargis storm surge in Myanmar. Nat. Geosci. *2*, 448–449.
18. Neumann, J., Emanuel, K., Ravela, S., Ludwig, L., and Verly, C. (2015). Risks of coastal storm surge and the effect of sea level rise in the Red River delta, Vietnam. Sustainability *7*, 6553–6572.
19. Scheiber, L., Sairam, N., Hoballah Jalloul, M., Rafiezadeh Shahi, K., Jordan, C., Visscher, J., Zadeh, T.E., Oostwegel, L.J.N., Schorlemmer, D., Son, N.T., et al. (2024). Effective adaptation options to alleviate nuisance flooding in coastal megacities—learning from Ho Chi Minh City, Vietnam. Earths Future *12*, e2024EF004766.
20. Qiu, J., Liu, B., Yang, F., Wang, X., and He, X. (2022). Quantitative stress test of compound coastal-fluvial floods in China's Pearl River delta. Earths Future *10*, e2021EF002638.
21. Du, H., Fei, K., and Gao, L. (2024). Nonlinear tide-river-surge interactions and their impacts on compound flooding during typhoon Hato in the Pearl River delta. JGR. Oceans *129*, e2023JC020673.
22. De Dominicis, M., Wolf, J., Jevrejeva, S., Zheng, P., and Hu, Z. (2020). Future interactions between sea level rise, tides, and storm surges in the world's largest urban area. Geophys. Res. Lett. *47*, e2020GL087002.
23. Emanuel, K., Ravela, S., Vivant, E., and Risi, C. (2006). A statistical deterministic approach to hurricane risk assessment. Bull. Am. Meteorol. Soc. *87*, 299–314.
24. Emanuel, K., Sundararajan, R., and Williams, J. (2008). Hurricanes and global warming: Results from downscaling IPCC AR4 simulations. Bull. Am. Meteorol. Soc. *89*, 347–368.

25. Lee, C.Y., Tippett, M.K., Sobel, A.H., and Camargo, S.J. (2018). An environmentally forced tropical cyclone hazard model. J. Adv. Model. Earth Syst. *10*, 223–241.

26. Bloemendaal, N., Haigh, I.D., de Moel, H., Muis, S., Haarsma, R.J., and Aerts, J.C.J.H. (2020). Generation of a global synthetic tropical cyclone hazard dataset using storm. Sci. Data *7*, 40.

27. Jing, R., and Lin, N. (2020). An environment-dependent probabilistic tropical cyclone model. J. Adv. Model. Earth Syst. *12*, e2019MS001975.

28. Leijnse, T.W.B., Giardino, A., Nederhoff, K., and Caires, S. (2022). Generating reliable estimates of tropical-cyclone-induced coastal hazards along the bay of bengal for current and future climates using synthetic tracks. Nat. Hazards Earth Syst. Sci. *22*, 1863–1891.

29. Lin, N., Lane, P., Emanuel, K.A., Sullivan, R.M., and Donnelly, J.P. (2014). Heightened hurricane surge risk in northwest florida revealed from climatological-hydrodynamic modeling and paleorecord reconstruction. JGR. Atmospheres *119*, 8606–8623.

30. Garner, A.J., Mann, M.E., Emanuel, K.A., Kopp, R.E., Lin, N., Alley, R.B., Horton, B.P., DeConto, R.M., Donnelly, J.P., and Pollard, D. (2017). Impact of climate change on New York City's coastal flood hazard: Increasing flood heights from the preindustrial to 2300 CE. Proc. Natl. Acad. Sci. USA *114*, 11861–11866.

31. Yin, J., Lin, N., Yang, Y., Pringle, W.J., Tan, J., Westerink, J.J., and Yu, D. (2021). Hazard assessment for typhoon-induced coastal flooding and inundation in Shanghai, China. JGR. Oceans *126*, e2021JC017319.

32. Meiler, S., Vogt, T., Bloemendaal, N., Ciullo, A., Lee, C.Y., Camargo, S.J., Emanuel, K., and Bresch, D.N. (2022). Intercomparison of regional loss estimates from global synthetic tropical cyclone models. Nat. Commun. *13*, 6156.

33. Khan, M.J.U., Durand, F., Emanuel, K., Krien, Y., Testut, L., and Islam, A.K.M.S. (2022). Storm surge hazard over bengal delta: a probabilistic–deterministic modelling approach. Nat. Hazards Earth Syst. Sci. *22*, 2359–2379.

34. Storm surge and wave modelling: Present and future conditions Research and Analysis of Bangladesh Coastal Zone (Sustainable Polders Adapted to Coastal Dynamics) contract. Consultant Firms: DHI, Deltares, IWM, Columbia University, Colorado University, IHE Delft. Tech. Rep. Bangladesh Water Development Board and Ministry of Water Resources 2022. http://ceip-bwdb.gov.bd/Tech_Report/LTM/June22(3).pdf.

35. Luettich, R.A., Westerink, J.J., and Scheffner, N.W. (1992). Adcirc: an advanced three-dimensional circulation model for shelves, coasts, and estuaries. Report 1, theory and methodology of Adcirc-2dd1 and Adcirc-3dl (Tech. Rep. U.S. Army Corps of Engineers, Waterways Experiment Station). https://apps.dtic.mil/sti/tr/pdf/ADA261608.pdf.

36. Krien, Y., Mayet, C., Testut, L., Durand, F., Tazkia, A.R., Islam, A.K.M.S., Gopalakrishna, V.V., Becker, M., Calmant, S., Shum, C.K., et al. (2016). Improved bathymetric dataset and tidal model for the northern Bay of Bengal. Mar. Geod. *39*, 422–438.

37. Frank, N.L., and Husain, S.A. (1971). The deadliest tropical cyclone in history? Bull. Am. Meteorol. Soc. *52*, 438–445.

38. As-Salek, J.A. (1998). Coastal trapping and funneling effects on storm surges in the Meghna estuary in relation to cyclones hitting Noakhali–Cox's Bazar coast of Bangladesh. J. Phys. Oceanogr. *28*, 227–249.

39. Wu, Z., Hu, C., Lin, L., Chen, W., Huang, L., Lin, Z., and Yang, S. (2023). Unraveling the strong covariability of tropical cyclone activity between the Bay of Bengal and the South China Sea. npj Clim. Atmos. Sci. *6*, 180.

40. Philip, S., Sparrow, S., Kew, S.F., Van Der Wiel, K., Wanders, N., Singh, R., Hassan, A., Mohammed, K., Javid, H., Haustein, K., et al. (2019). Attributing the 2017 Bangladesh floods from meteorological and hydrological perspectives. Hydrol. Earth Syst. Sci. *23*, 1409–1429.

41. Han, S.C., Ghobadi-Far, K., Yeo, I.Y., McCullough, C.M., Lee, E., and Sauber, J. (2021). Grace follow-on revealed Bangladesh was flooded early in the 2020 monsoon season due to premature soil saturation. Proc. Natl. Acad. Sci. USA *118*, e2109086118.

42. Jakobsen, F., Azam, M.H., Ahmed, M.M.Z., and Mahboob-ul Kabir, M. (2006). Cyclone storm surge levels along the Bangladeshi coastline in 1876 and 1960–2000. Coast. Eng. J. *48*, 295–307.

43. Zelinka, M.D., Myers, T.A., McCoy, D.T., Po-Chedley, S., Caldwell, P.M., Ceppi, P., Klein, S.A., and Taylor, K.E. (2020). Causes of higher climate sensitivity in cmip6 models. Geophys. Res. Lett. *47*, e2019GL085782.

44. Meehl, G.A., Senior, C.A., Eyring, V., Flato, G., Lamarque, J.F., Stouffer, R.J., Taylor, K.E., and Schlund, M. (2020). Context for interpreting equilibrium climate sensitivity and transient climate response from the cmip6 earth system models. Sci. Adv. *6*, eaba1981.

45. Bakker, T.M., Antolínez, J.A.A., Leijnse, T.W.B., Pearson, S.G., and Giardino, A. (2022). Estimating tropical cyclone-induced wind, waves, and surge: A general methodology based on representative tracks. Coast. Eng. *176*, 104154.

46. Krien, Y., Testut, L., Islam, A.k.m.s., Bertin, X., Durand, F., Mayet, C., Tazkia, A.r., Becker, M., Calmant, S., Papa, F., et al. (2017). Towards improved storm surge models in the northern Bay of Bengal. Cont. Shelf Res. *135*, 58–73.

47. Wang, X., and Jiang, H. (2024). Physics-guided deep learning for skillful wind-wave modeling. Sci. Adv. *10*, eadr3559.

48. Knutson, T., Camargo, S.J., Chan, J.C.L., Emanuel, K., Ho, C.H., Kossin, J., Mohapatra, M., Satoh, M., Sugi, M., Walsh, K., and Wu, L. (2020). Tropical cyclones and climate change assessment: Part II: Projected response to anthropogenic warming. Bull. Am. Meteorol. Soc. *101*, E303–E322.

49. Kopp, R.E., Oppenheimer, M., O'Reilly, J.L., Drijfhout, S.S., Edwards, T.L., Fox-Kemper, B., Garner, G.G., Golledge, N.R., Hermans, T.H., Hewitt, H.T., et al. (2023). Communicating future sea-level rise uncertainty and ambiguity to assessment users. Nat. Clim. Change *13*, 648–660.

50. Matthews, T., Wilby, R.L., and Murphy, C. (2019). An emerging tropical cyclone–deadly heat compound hazard. Nat. Clim. Change *9*, 602–606.

51. Merz, B., Blöschl, G., Vorogushyn, S., Dottori, F., Aerts, J.C.J.H., Bates, P., Bertola, M., Kemter, M., Kreibich, H., Lall, U., and Macdonald, E. (2021). Causes, impacts and patterns of disastrous river floods. Nat. Rev. Earth Environ. *2*, 592–609.

52. Bates, P.D., Quinn, N., Sampson, C., Smith, A., Wing, O., Sosa, J., Savage, J., Olcese, G., Neal, J., Schumann, G., et al. (2021). Combined modeling of us fluvial, pluvial, and coastal flood hazard under current and future climates. Water Resour. Res. *57*, e2020WR028673.

53. Leijnse, T., van Ormondt, M., Nederhoff, K., and van Dongeren, A. (2021). Modeling compound flooding in coastal systems using a computationally efficient reduced-physics solver: Including fluvial, pluvial, tidal, wind-and wave-driven processes. Coast. Eng. *163*, 103796.

54. Paszkowski, A., Goodbred, S., Jr, Borgomeo, E., Khan, M.S.A., and Hall, J.W. (2021). Geomorphic change in the Ganges–Brahmaputra–Meghna delta. Nat. Rev. Earth Environ. *2*, 763–780.

55. Nienhuis, J.H., Ashton, A.D., Edmonds, D.A., Hoitink, A.J.F., Kettner, A.J., Rowland, J.C., and Törnqvist, T.E. (2020). Global-scale human impact on delta morphology has led to net land area gain. Nature *577*, 514–518.

56. Becker, M., Seeger, K., Paszkowski, A., Marcos, M., Papa, F., Almar, R., Bates, P., France-Lanord, C., Hossain, M.S., Khan, M.J.U., et al. (2024). Coastal flooding in Asian megadeltas: Recent advances, persistent challenges, and call for actions amidst local and global changes. Rev. Geophys. *62*, e2024RG000846.

57. Calafat, F.M., and Marcos, M. (2020). Probabilistic reanalysis of storm surge extremes in Europe. Proc. Natl. Acad. Sci. USA *117*, 1877–1883.

58. Holland, G.J. (1982). Tropical cyclone motion: environmental interacton plus a beta efect. https://doi.org/10.1175/1520-0469(1983)040<0328:TCMEIP>2.0.CO;2. https://journals.ametsoc.org/view/journals/atsc/40/2/1520-0469_1983_040_0328_tcmeip_2_0_co_2.xml.

59. Emanuel, K., DesAutels, C., Holloway, C., and Korty, R. (2004). Environmental control of tropical cyclone intensity. J. Atmos. Sci. *61*, 843–858.

60. Westerink, J.J., Luettich, R.A., Jr, Blain, C.A., and Scheffner, N.W. (1994). Adcirc: an advanced three-dimensional circulation model for shelves,

coasts, and estuaries. Report 2. User's manual for Adcirc-2ddi. Tech. Rep. U.S. Army Corps of Engineers, Waterways Experiment Station. https://apps.dtic.mil/sti/tr/pdf/ADA276150.pdf.

61. Pringle, W.J., Wirasaet, D., Roberts, K.J., and Westerink, J.J. (2021). Global storm tide modeling with Adcirc v55: unstructured mesh design and performance. Geosci. Model Dev. (GMD) *14*, 1125–1145.
62. Roberts, K.J., Pringle, W.J., and Westerink, J.J. (2019). Oceanmesh2d 1.0: Matlab-based software for two-dimensional unstructured mesh generation in coastal ocean modeling. Geosci. Model Dev. (GMD) *12*, 1847–1868.
63. Roberts, K.J., Pringle, W.J., Westerink, J.J., Contreras, M.T., and Wirasaet, D. (2019). On the automatic and a priori design of unstructured mesh resolution for coastal ocean circulation models. Ocean Model. *144*, 101509.
64. Wessel, P., and Smith, W.H.F. (1996). A global, self-consistent, hierarchical, high-resolution shoreline database. J. Geophys. Res. *101*, 8741–8743.
65. Weatherall, P., Marks, K.M., Jakobsson, M., Schmitt, T., Tani, S., Arndt, J.E., Rovere, M., Chayes, D., Ferrini, V., and Wigley, R. (2015). A new digital bathymetric model of the world's oceans. Earth Space Sci. *2*, 331–345.
66. Yamazaki, D., Ikeshima, D., Tawatari, R., Yamaguchi, T., O'Loughlin, F., Neal, J.C., Sampson, C.C., Kanae, S., and Bates, P.D. (2017). A high-accuracy map of global terrain elevations. Geophys. Res. Lett. *44*, 5844–5853.
67. Lin, P., Pan, M., Allen, G.H., de Frasson, R.P., Zeng, Z., Yamazaki, D., and Wood, E.F. (2020). Global estimates of reach-level bankfull river width leveraging big data geospatial analysis. Geophys. Res. Lett. *47*, e2019GL086405.
68. Tazkia, A.r., Krien, Y., Durand, F., Testut, L., Islam, A.S., Papa, F., and Bertin, X. (2017). Seasonal modulation of m2 tide in the northern Bay of Bengal. Cont. Shelf Res. *137*, 154–162.
69. Chavas, D.R., Lin, N., and Emanuel, K. (2015). A model for the complete radial structure of the tropical cyclone wind field. Part I: Comparison with observed structure. J. Atmos. Sci. *72*, 3647–3662.
70. Emanuel, K. (2004). Tropical cyclone energetics and structure. Atmospheric Turbulence and Mesoscale Meteorology *165*, 192.
71. Emanuel, K., and Rotunno, R. (2011). Self-stratification of tropical cyclone outflow. part i: Implications for storm structure. J. Atmos. Sci. *68*, 2236–2249.
72. Lin, N., and Chavas, D. (2012). On hurricane parametric wind and applications in storm surge modeling. J. Geophys. Res. *117*.
73. Bretschneider, C.L. (1972). A non-dimensional stationary hurricane wave model. In Offshore Technology Conference (OTC), pp. OTC-1517. https://doi.org/10.4043/1517-MS.
74. Powell, M.D., Houston, S.H., and Reinhold, T.A. (1996). Hurricane Andrew's landfall in South Florida. Part I: Standardizing measurements for documentation of surface wind fields. Weather Forecast. *11*, 304–328.
75. Holland, G.J. (1980). An analytic model of the wind and pressure profiles in hurricanes. Mon. Weather Rev. *108*, 1212–1218.
76. Powell, M.D., Vickery, P.J., and Reinhold, T.A. (2003). Reduced drag coefficient for high wind speeds in tropical cyclones. Nature *422*, 279–283.
77. Wang, S., Lin, N., and Gori, A. (2022). Investigation of tropical cyclone wind models with application to storm tide simulations. JGR Atmospheres *127*, e2021JD036359.
78. Pringle, W.J., Wirasaet, D., and Westerink, J.J. (2018). Modifications to internal tide conversion parameterizations and implementation into barotropic ocean models. Preprint at EarthArXiv. https://doi.org/10.31223/osf.io/84w53.
79. Shihora, L., Sulzbach, R., Dobslaw, H., and Thomas, M. (2022). Self-attraction and loading feedback on ocean dynamics in both shallow water equations and primitive equations. Ocean Model. *169*, 101914.
80. Egbert, G.D., and Erofeeva, S.Y. (2002). Efficient inverse modeling of barotropic ocean tides. J. Atmos. Ocean. Technol. *19*, 183–204.
81. Lyard, F.H., Allain, D.J., Cancet, M., Carrère, L., and Picot, N. (2021). Fes2014 global ocean tide atlas: design and performance. Ocean Sci. *17*, 615–649.
82. Blakely, C.P., Ling, G., Pringle, W.J., Contreras, M.T., Wirasaet, D., Westerink, J.J., Moghimi, S., Seroka, G., Shi, L., Myers, E., et al. (2022). Dissipation and bathymetric sensitivities in an unstructured mesh global tidal model. JGR Oceans *127*, e2021JC018178.
83. Islam, M.S., Akter, E., Debnath, P., Islam, Md.S., and Bin Ali, A.A. (2021). Characteristics of sediment in the inner shelf zone of Bangladesh. BMJ Special Issue on Coastal and Marine Geoscience *1*, 179–190.
84. Pringle, W.J., Wirasaet, D., Suhardjo, A., Meixner, J., Westerink, J.J., Kennedy, A.B., and Nong, S. (2018). Finite-element barotropic model for the indian and western pacific oceans: Tidal model-data comparisons and sensitivities. Ocean Model. *129*, 13–38.
85. Ngodock, H.E., Souopgui, I., Wallcraft, A.J., Richman, J.G., Shriver, J.F., and Arbic, B.K. (2016). On improving the accuracy of the m2 barotropic tides embedded in a high-resolution global ocean circulation model. Ocean Model. *97*, 16–26.
86. Sindhu, B., and Unnikrishnan, A.S. (2013). Characteristics of tides in the Bay of Bengal. Mar. Geod. *36*, 377–407.
87. Rose, L., and Bhaskaran, P.K. (2022). Tidal variations associated with sea level changes in the northern Bay of Bengal. Estuar. Coast Shelf Sci. *272*, 107881.
88. ITJSCE (2008). Investigation Report on the Storm Surge Disaster by Cyclone Sidr in November 2007 in Bangladesh. Tech. Rep. Japan Society of Civil Engineers. https://www.jsce.or.jp/report/46/files/Bangladesh_Investigation.pdf.
89. Mamnun, N., Bricheno, L.M., and Rashed-Un-Nabi, M. (2020). Forcing ocean model with atmospheric model outputs to simulate storm surge in the Bangladesh coast. Trop. Cycl. Res. Rev. *9*, 117–134.
90. Kopp, R.E., Garner, G.G., Hermans, T.H.J., Jha, S., Kumar, P., Reedy, A., Slangen, A.B.A., Turilli, M., Edwards, T.L., Gregory, J.M., et al. (2023). The Framework for Assessing Changes To Sea-level (FACTS) v1.0: a platform for characterizing parametric and structural uncertainty in future global, relative, and extreme sea-level change. Geosci. Model Dev. *16*, 7461–7489. https://doi.org/10.5194/gmd-16-7461-2023.
91. Marsooli, R., Lin, N., Emanuel, K., and Feng, K. (2019). Climate change exacerbates hurricane flood hazards along US Atlantic and Gulf coasts in spatially varying patterns. Nat. Commun. *10*, 3785.
92. Moftakhari, H.R., Salvadori, G., AghaKouchak, A., Sanders, B.F., and Matthew, R.A. (2017). Compounding effects of sea level rise and fluvial flooding. Proc. Natl. Acad. Sci. USA *114*, 9785–9790.
93. Lin, N., Emanuel, K., Oppenheimer, M., and Vanmarcke, E. (2012). Physically based assessment of hurricane surge threat under climate change. Nat. Clim. Change *2*, 462–467.
94. Coles, S. (2001). An Introduction to Statistical Modeling of Extreme Values, *208* (London: Springer Series in Statistics)978-1-85233-459-8. https://doi.org/10.1007/978-1-4471-3675-0.
95. Terrell, G.R., and Scott, D.W. (1992). Variable kernel density estimation. Ann. Stat. *20*, 1236–1265.
96. Bhardwaj, P., and Singh, O. (2020). Climatological characteristics of Bay of Bengal tropical cyclones: 1972–2017. Theor. Appl. Climatol. *139*, 615–629.
97. Emanuel, K. (2022). Tropical cyclone seeds, transition probabilities, and genesis. J. Clim. *35*, 3557–3566.
98. Cannon, A.J., Sobie, S.R., and Murdock, T.Q. (2015). Bias correction of GCM precipitation by quantile mapping: how well do methods preserve changes in quantiles and extremes? J. Clim. *28*, 6938–6959.
99. Gori, A., Lin, N., Xi, D., and Emanuel, K. (2022). Tropical cyclone climatology change greatly exacerbates us extreme rainfall–surge hazard. Nat. Clim. Change *12*, 171–178.